Towards global indicator of durability performance and carbon footprint of clinker-slag-limestone cement-based concrete exposed to carbonation

Imane Elkhaldi, Emmanuel Rozière, Philippe Turcry, Ahmed Loukili

Towards global indicator of durability performance and carbon footprint of clinker-slag-limestone cement-based concrete exposed to carbonation

Imane ELKHALDI[1,2], Emmanuel ROZIERE[1*], Philippe Turcry[3], Ahmed LOUKILI[1]

[1] Institut de recherche en génie civil et mécanique, UMR CNRS 6183, Ecole Centrale de Nantes, 44321, Nantes cedex 3, France

[2] Edycem, Rue du Fléchet, 85600 Boufféré, France

[3] La Rochelle University, LaSIE UMR CNRS 7356, Avenue Michel Crepeau, 17042, La Rochelle Cedex 1, France

* Corresponding author, emmanuel.roziere@ec-nantes.fr

Abstract

This article aims at defining an effective global warming potential criterion for qualifying a concrete mixture based on a CO_2 calculation and durability performance tests, as well as understanding the parameters that influence the duration of initiation and propagation of corrosion in concretes exposed to carbonation-induced corrosion. An experimental study was conducted in order to assess the resistance to carbonation and the electrical resistivity for concretes made of multi-composite cements with ground-granulated blast furnace slag (GGBS) and limestone in the limits of new cement European standard EN 197-5, and to understand the link between these properties and the composition of the cements. A model is presented which allows to predict the service life of the concrete cover from the material data of the concrete (accelerated carbonation rate, electrical resistivity), environmental parameters (HR, T, CO_2) and minimum cover. It was found that the reactive CaO content of cements influences the carbonation rate of concrete, and the electrical resistivity and the GGBS content of cements were found to have a good correlation. The model used allows comparing the studied cements from the CO_2 emission/service life ratios.

Keywords: Slag; Limestone; Durability; Carbonation; Resistivity; CO_2

1- Introduction

The greenhouse gases emissions (GHGE) of building sector have two main causes: the energy used for heating, cooling, and lighting the buildings and the production of construction materials. Historically, environmental regulations have first focused on energy efficiency of buildings by reducing their energy consumption but the recent regulations, such as French environmental regulation RE2020, also set targets the GHGE associated to materials throughout their whole life cycle. This performance objective is called E+C- (Ministry for the ecological and solidary transition, 2020), as the energy efficiency must be improved and the carbon footprint should be reduced by using construction materials with low environmental impact. Thus, research works are recently moving towards exploring ways to reduce carbon emissions of concrete, which is the most widely used construction material. Cement is responsible for more than 75% of the carbon emissions of concrete from its manufacturing phase to its placement (Di Filippo et al., 2019). This is mainly due to clinker production which is both energy-intensive and polluting. The CO_2 emissions related to the production of cement represent 4 to 5% of all greenhouse gases produced worldwide in 2019 (IPCC, 2022). Nonetheless, normatively speaking, there is no regulatory definition of "low-carbon concrete". In the literature, several indicators have been defined, such as the carbon cost of 1 MPa compressive strength in (Bolte et al., 2019). This has also been designated by CO_2 efficiency to characterize low carbon concrete (Yang et al., 2017). This concept is interesting as it takes into account the performance of the concrete that represents its functional unit from a life cycle analysis (LCA) point of view. However, it does not take into account the durability aspect of concrete, which is equally important. The long term performance of concrete is actually an important factor to consider since maintenance work on reinforced concrete structures induces a significant carbon cost which is added to the primary carbon cost of the structure (Gartner, 2004).

Compressive strength is not a fully satisfactory durability indicator, as it cannot provide a reliable estimation of the service life (SL) duration of reinforced concrete structures, which depends on several factors, especially environmental actions. In the current concrete standard in Europe (EN 206-1), the environmental conditions are represented by the exposure class. For the general case of buildings, which are neither close to the sea nor exposed to chemical attacks, the most considered exposure class is XC class (XC1 to XC4) which concerns concretes subjected to the risk of corrosion induced by carbonation The environnemental conditions concerned by this exposure class are described in table 1.

Table 1: Environmental conditions described by XC exposure class

	Description of the environment
XC1	Permanently dry or wet
XC2	Wet, rarely dry
XC3	Moderate humidity
XC4	Alternating wet and dry

This standard includes deemed-to-satisfy provisions, i.e. for each class the maximum W/C ratio, the minimum cement content as well as requirements on the contents of mineral additions (MAs) which can be used as a MA as a replacement of Portland cement with a high clinker content (> 80%). To deviate from these prescriptions, it remains possible to use performance-based specifications (Rozière et al., 2009)**.**

In parallel with the new environmental regulation, the new cement standard EN 197-5 (2021) has also been published. It describes two categories of ternary cements with lower clinker contents, namely Portland CEM II/C-M cements that incorporates a higher percentage of MAs (up to 50%) than existing CEM II Portland cements, and a new category of cements which is CEM VI with a clinker content ranging from 35 to 49%. This standard aims at facilitating the integration of cements with low clinker content into the market by including them in a regulatory framework. However, as long as "low-carbon concrete" has not been defined, it cannot be said that CEM II/C-M and CEM VI are "low-carbon cements"; it actually depend on the durability of concretes made with these cements.

Ternary cements based on a MA rich in reactive silico-aluminates, such as metakaolin and ground granulated blast furnace slag (GGBS) have been the subject of many research works recently (Arumugam, 2022). The particular interest in these binders lies in their great potential to maximize the clinker replacement rate (Proske et al., 2018). The synergy between aluminates and limestone enhances the mechanical properties in the short and long term. The nucleation effect of limestone powder actually accelerates the hydration of the clinker at early age (Palm et al., 2016), and the GGBS, given its latent hydraulicity and its pozzolanic properties, improves the mechanical properties in the long term (Giergiczny, 2019). In addition, the reaction of the calcium carbonates with the aluminates from the clinker and the GGBS, stabilizes ettringite and carboaluminates, which densifies the microstructure

(Matschei et al., 2007). The hydration and microstructure of this type of binders has been largely studied in the literature (Adu-Amankwah, 2016).

However, few data can be found on the durability of concrete based on these cements with respect to corrosion induced by carbonation. The carbonation risk of these binders has been studied in (Bolte et al., 2019) and (Proske et al., 2018). In both papers, it was shown that the carbonation resistance of concrete containing composite cements is similar to that of concrete made with CEM III/A GGBS cements with the same mechanical strength but remains low compared to Portland cement. The carbonation rate has been found to be inversely proportional to the clinker content of the cements (Bolte et al., 2019). The resistance to carbonation is an important parameter since it provides information on the initiation phase of corrosion, but remains insufficient to quantify the service life of concrete structures with respect to corrosion induced by carbonation. The corrosion propagation phase is actually significant under certain environmental conditions (Farissi, 2020; Tuutti, 1982). According to (Tuutti, 1982) , this phase depends on the electrical resistivity of the concrete which provides information on the corrosion rate of the reinforcements (Andrade, 2010). Data on the electrical resistivity (ρ) or the conductivity ($1/\rho$) of cementitious materials containing GGBS have been published (Alonso et al., 2012), but there are very few published data about electrical resistivity of concretes containing clinker-GGBS-limestone (K-S-LL) multi-composite cements.

This article deals with the ternary cements K-S-LL within the scope of the new cement European standard EN 197-5. The approach of this study aims at evaluating the service life duration, the CO_2 emissions related to the production of concretes made up with K-S-LL cements and binary limestone and GGBS cements respectively. The purpose of the experimental study is to assess the influence of durability parameters on the SL of concrete exposed to carbonation-induced corrosion, namely carbonation resistance and electrical resistivity, as well as to understand the link between those properties and cement composition. The results are incorporated into an empirical model to predict the service life of the concretes studied. The ratio of the CO_2 emissions related to the production of concrete to the service life will be used as a new indicator to estimate the interest in using the new cements.

2- Experimental program and procedures

2.1. Materials and mixtures

The ternary cements were manufactured in the laboratory using a V-shaped rotary mixer from four powders: ordinary Portland cement (CEM I), limestone Portland cement (CEM II/B-LL) with a limestone filler (LL) content of 30% by mass, ground granulated blast furnace GGBS (GGBS), and gypsum. CEM I and CEMII/B-LL were commercial cements made with the same clinker (K). The chemical composition and the physical properties of the raw materials are given in table 2. The particle size distribution of the raw materials are given in figure 2.

Table 2: Chemical and physical properties of the raw powders

	CEM I	CEMII/B-LL	GGBS
Chemical Composition [%]			
CaO	63.6	60.4	41.6
SiO_2	20.1	15.9	35.9
Al_2O_3	4.4	3.4	11.7
Fe_2O_3	2.2	1.7	0.5
SO_3	3.3	2.9	0.1
MgO	4	3.1	7.4
TiO_2	0.2	-	0.7
S--	0.02	-	0.7
Na_2Oeq	0.6	0.42	0.58
Loss On Ignition (LOI)	1.4	12.5	-
Clinker percentage (%)	100	70	-
Clinker Mineralogical composition [%]			
C_3S	67	68	-
C_2S	11	10	-
C_3A	9	9	-
C_4AF	7	7	-
Gypsum	4.9	4.9	-
Physical and mechanical properties			
Density	3.14	3.01	2.9
Blaine surface [cm^2/g]	4882	5168	>4200
Time of initial setting	1h55	2h36	-
f_{c2j} (MPa)	44	25	-
f_{c28j} (MPa)	63	44	-

The $CaCO_3$ content of limestone in CEM II/B-LL was 95.5%. Additional gypsum was incorporated in order to reach a Calcium sulfate/(Clinker+GGBS) ratio of at least 3% to have enough calcium sulphate to control the short-term hydration of the aluminates contained in both clinker and GGBS. The gypsum was the same as included in CEM I and CEM II/B-LL.

The compositions of studied cements are shown in table 3 and on the K-S-LL ternary diagram of figure 1. This diagram also includes the boundaries of new CEM II/C (green zone) and CEM VI (yellow zone) cements defined in standard EN 197-5 (EN 197-5:2021). The raw materials were proportioned by mass in order to obtain four different binders: 2 ternary binders C1 (CEM VI) and C3 (limit between CEM II/C and CEM VI), and 2 conventional binary cements, CEM II, limestone Portland cement, widely used today, and CEM III, which comply with the existing cement standard EN 197-1. CEM II and CEM III are used as references to evaluate the relevance of the new ternary cements. C1 and C3 have the same Limestone/Clinker (LL/K) ratio of 0.4, a preliminary study on 15 ternary cements showed that C1 and C3 cements had the same strength on standardized mortar from 7 days, and both concrete had the same characteristic strength (table 5). C1 and CEM III have the same clinker content with 15% of the slag substituted in limestone for C1. Studying these two cements allows to study the effect of limestone on the durability of concrete based on ternary cements with high clinker replacement.

Table 3: Composition of the studied cements (mass proportions)

Mix designation	Clinker	GGBS	Limestone	LL/K
CEM II	90	0	10	0.11
CEM III	35	65	0	0
C1	35	50	15	0.43
C3	50	30	20	0.40

The homogeneity of the powders prepared was confirmed using X-ray fluorescence spectrometry (XRF) analysis by determining the atomic composition of the raw and mixed powders. The theoretical composition calculated from the measured composition of the raw powders was compared to the actual measured composition of the mixed ones. The relative errors found were small especially for the preponderant elements, namely Ca and Si (maximum error < 2%)

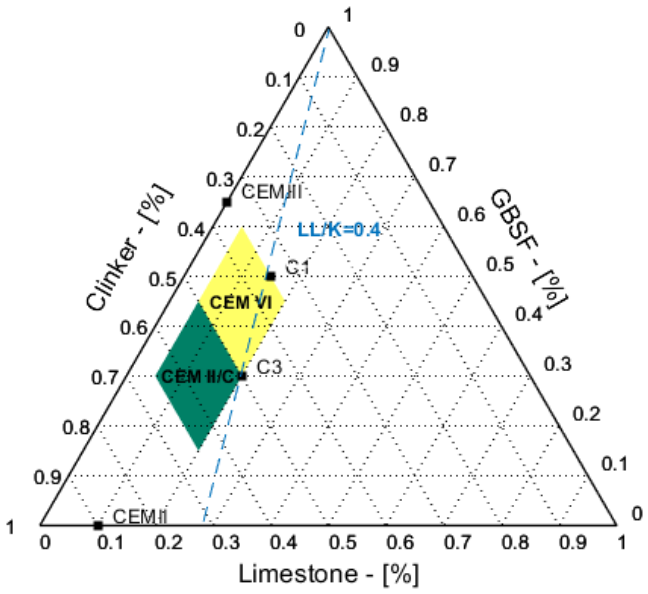

157

158 **Figure 1: Studied cements, and boundaries of new ternary cements CEM II/C and CEM VI**

159

160 Four concrete mixtures were designed keeping all the mass ratios constant; only the cement
161 composition varied. The properties of aggregates are given in Table 4. The particle size
162 distribution of the aggregates used is given in figure 2. A polycarboxylate-type plasticizer
163 showing a good compatibility with the binders studied was used. The plasticizer content was
164 adjusted to reach around 150 mm slump of fresh concrete. The compositions of concrete
165 mixtures comply with the requirements of the NF 206/CN standard with regard to the
166 maximum W/C ratios (0.65 and 0.60), the minimum cement content (260 and 280 kg/m^3) for
167 XC1-XC2 and XC3-XC4 exposure classes respectively. It is noteworthy that the compressive
168 strengths obtained at 28 days comply with the minium strength classes of 20 and 25 MPa
169 characteristic compressive strength respectively. The maximum aggregate size was 10 mm.
170 The concrete mixtures and proprerties are given in table 5 with f_{ck} the characteristic
171 compressive strength.

172

173 **Table 4: Physical properties of the aggregates**

Mix designation	Sand 0/4	Sand 0/2	Gravel 6.3/10
Mineralogy	Siliceous rolled sand	Amphibolite crushed sand	Amphibolite crushed gravel
Water absorption (%)	0.40	0.50	0.60
Density (kg/m^3)	2620	2960	2960

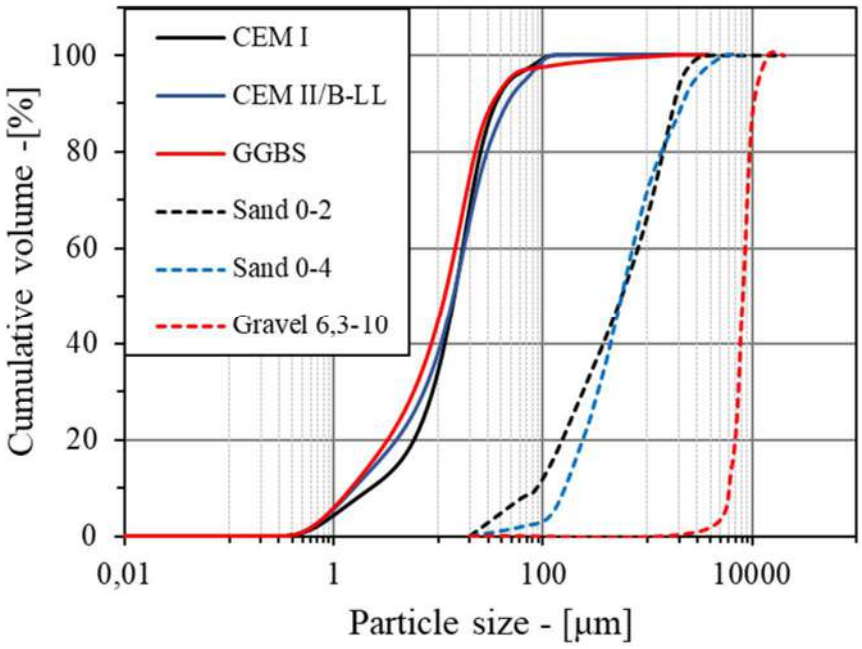

174

175 **Figure 2: Particle size distribution of the raw powders and aggregates**

176

177 **Table 5: Mixture composition (in kg/m^3) and properties of the studied concretes**

	CEM II	CEM III	C1	C3
Sand 0/4		434		
Sand 0/2		424		
Gravel 6,3/10		1051		
Cement		313		
Water		188		
Plasticizer (%)	0.3	0.3	0.45	0.45
Paste volume (l)	292	290	290	291
W/C		0.60		
f_{ck} (MPa)$^{(*)}$	40.2	32.7	25.3	25.4

178 $^{(*)}$ fck is the characteristic strength deduced from the average 28d strength according to
179 Eurocode 2.

180 ## 2.2. Experimental program

181 The concrete and cement pastes prepared have the same W/C ratio. The concrete specimens
182 were demolded after 24 hours and kept in water for 90 days in a room at 20 °C. Six
183 cylindrical concrete specimens of Ø110*220 mm^3 were manufactured for the accelerated
184 carbonation test and three cubic specimens of 150*150*150 mm^3 size for the electrical
185 resistivity tests.

Cylindrical cement paste samples of Ø25*50 mm^3 dimensions were prepared with the same W/C and cement composition as the studied concretes. Xanthan gum, which is a polysaccharide-based viscosity modifying admixture, was added to the cement paste to limit bleeding at proportions ranging from 0.6 to 1 wt% to the liquid fraction; as it was found to have limited effect on binders reactivity and cement hydration and therefore can be considered inert (Aboulayt et al., 2018). Xanthan gum was used at a constant W/C ratio. The cement pastes were demolded after 24 hours and kept in water in a room at 20 °C for 90 days to guarantee a degree of maturity comparable to the cement paste contained in the concretes. One paste sample was used to assess the microstructure of sound cement paste and another one was carbonated.

2.2.1. Durability tests:

a) Accelerated carbonation test

The accelerated carbonation testing procedure was adapted from European standard prCEN/TS 12390-12 to increase its sensitivity to materials performance (Turcry et al., 2019). The samples were obtained by sawing in two Φ110*220 mm^3 specimens; the lower and upper part of the sample were covered by adhesive aluminum to allow lateral carbonation. Subsequently, the specimens underwent the following pre-treatment to promote optimal conditions to accelerate carbonation:

- Drying at 45 °C +/- 5 °C with 3 specimens of standardized mortar 40*40*160 mm^3 made of CEM II/A-L prepared 35 days before the start date of drying. Drying lasts a minimum of 14 days until the mass loss of the control mortar specimens reaches at least 5.5%.

- Humidification in a climatic room at 20 °C and 52% RH for 7 days.

The interest of these two steps is to ensure optimal carbonation conditions. The drying step favours the CO_2 diffusion through concrete porous netwok, then humidification results in higher water saturation in the external part of the samples, which restores an aqueous phase in the porosity allowing carbonation reactions to take place. After preconditioning, the samples were placed in a carbonation chamber at 20 °C, 65% RH and 3% CO_2. The carbonation rate was estimated by monitoring the progress of the carbonation front at 0, 28, 42, and 70 days using phenolphthalein, on 3 specimens split in two.

For the cement pastes samples, the sample used for carbonation was cut into thin discs about 5 mm thick to be carbonated in the same conditions as concrete specimens. Before putting

them in the carbonation chamber (20°C, 65% RH, 3% CO_2), these discs were dried for 2 hours at 40°C and placed in a room at 20°C and 50% RH for 24h to ensure optimal carbonation conditions without altering their phase composition. The carbonation time was 42 days for all cement pastes. At the end of this period, a phenolphthalein test was carried out on a fragment of disc to check the complete carbonation of the disc.

b) Electrical resistivity

The measurements were carried out on three cylindrical Ø75*70 mm^3 specimens cored in the middle of cubic concrete samples and cut in two. The device consists of two halves insulating cylinders with 5 ring-electrodes equally spaced along the height (du Plooy et al., 2013). Figure 3 shows the arrangement of the electrodes and the measurement points. This configuration allows 4 measurement points on different slices of the sample and accounts for any heterogeneities. Indeed, it has been reported that the configuration with 4 measurement points gives more reliable results than that with two points (Hornbostel et al., 2013). The current is injected through two stainless steel disk electrodes, and the current measurement is made between two ring-electrodes. The measurement cell is connected to a commercial resistivity meter (Syscal Pro, Iris instrument). The current injected is a square alternating current at a frequency of 4Hz. The electrical resistivity is given by equation 1.

$$\rho = G\frac{\Delta V}{I} \quad (1)$$

ρ: is the electrical resistivity in (Ω.m), ΔV (V) is the measured potential difference, I (A) is the injected current and G is the geometric coefficient which is equal to the section to length A/L ratio (m). A is the cross-sectional area of the specimen and L is the length of the specimen.

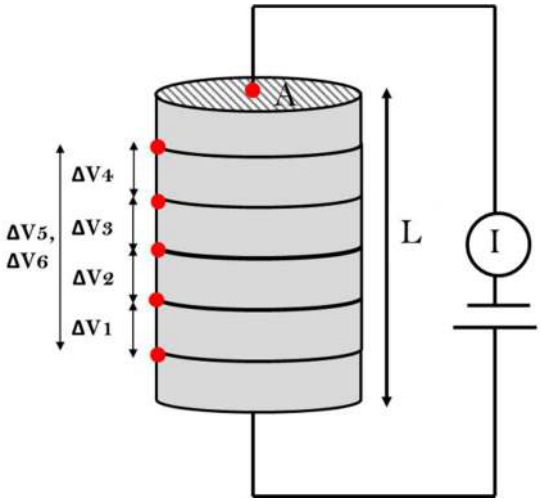

Figure 3: Schematic view of the resistivity measurement, adapted from (du Plooy et al., 2013)

The G coefficients for each measurement range are calculated by numerical modelling, the details are provided in (du Plooy et al., 2013).

2.2.2. Microstructural characterization

In order to assess the effect of hydration and carbonation on the pore size distribution (PSD), MIP analyses were performed on non-carbonated and carbonated concrete cubes. The cubes were cut from partially carbonated cylindrical Ø75*70 mm^3 specimens with a minimum carbonation depth of 13 mm. The non-carbonated samples were taken from the center and the carbonated one from the carbonated external layer.Measurements were carried out on with a Micromeritics AUTOPORE IV 9500 porosimeter at increasing pressures up to 400 MPa which corresponds to a minimum pore radius of 1.5 nm. The uncertainty on the threshold pore diameter was ±5% of the average value.

TGA analyses were performed on 50 mg sample of ground carbonated (C) and non carbonated (NC) cement pastes. Hydration was stopped before the test using isopropanol (Cardinaud et al., 2021). The temperature increased from 20 to 1000 °C at a rate of 10 °C/min. Water loss between 40 °C and 400 °C refers to bound water ($\mathbf{BW_{40\text{-}400°C}}$) and it is attributed to C-S-H, ettringite, AFm and carboaluminates decomposition. It is calculated using stepwise method and reported to anhydrous cement (equation 2). The CO_2 which decomposes from the initial limestone (Lini) present in the cement is added to the remaining mass after 900°C heating to obtain the anhydrous cement.:

$$m_{anh} = m_{900°C} + L_{ini}\frac{M_{CO_2}}{M_{CaCO_3}} \quad (2)$$

with: $m_{900°C}$ the weight at 900°C , L_{ini} the percentage of the initial limestone present in the cement, and M_{CO_2} and M_{CaCO_3} the molar masses of CO_2 and $CaCO_3$ which are equal to 44 g/mol and 100 g/mol respectively.

Water loss between 400°C and 550°C is attributed to portlandite decomposition. It was calculated using tangent method (Kocaba, 2009). The portlandite (**CH**) content was then calculated using the molar masses of CH and water. For non carbonated cement paste, CH content was corrected with the mass loss between 550 and 850 C corresponding to the CO_2 released by the decomposition of $CaCO_3$ formed from carbonated portlandite according to (Cardinaud et al., 2021). The total CH content was reported to the mass of anhydrous cement. The sum of the two water losses mentioned above refers to the total bound water (**$BW_{40\text{-}550°C}$**) which gives information about the hydration degree of the binder. The uncertainty on the CH content was ±4% of the average value, and the uncertainty on the **$BW_{40\text{-}550°C}$** content was ±2% of the average value.

XRD analysis was performed on carbonated and non carbonated ground cement pastes using a Malvern Panalytical Aeris instrument. Scanning program consisted in rotating between 7 and 70°2θ with a step size of 0.01°2θ and a 480.165 ms per step.

3- Service life prediction model

The service life (SL) of concrete structures is largely determined by the durability of its concrete cover, which protects steel reinforcement from the corrosion induced by environmental actions. Theoretically, the SL of the cover can be quantified based on the environment of the structure, the mechanisms that govern aggressive agent penetration, and the properties of the concrete.

According to the conceptual model of Tuutti (Tuutti, 1982) (figure 4) the SL of reinforced concrete structure can be divided into two phases: initiation and propagation phase.

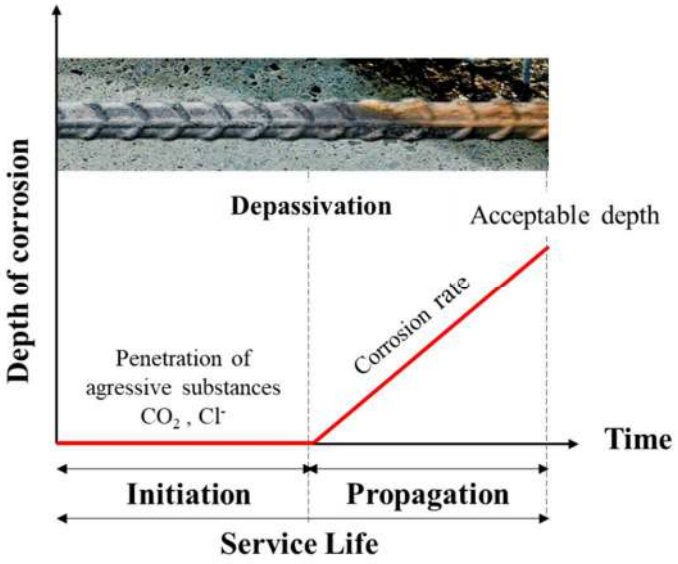

Figure 4: Service life phases according to Tuutti's model (Tuutti, 1982)

-The initiation phase characterizes the period when the aggressive agents (CO_2, Cl^-) penetrate the concrete cover and reach the reinforcement. This diffusion is accompanied by a change in the microstructure and the pore solution.

- The propagation phase: Corrosion does not occur totally once the carbonation front or chlorides reach the reinforcement. The reinforcement corrodes gradually until it reaches a critical corrosion depth (X_{crit}), which corresponds to a diameter loss and results in a crack opening on the concrete surface. For a fracture opening of 0.1 mm, there are empirical formulas that give X_{crit} (Torres-Acosta and Sagues, 2004). The propagation phase can be divided into several sub-periods describing different limit states (Markeset and Myrdal, 2008). In our study, we consider only the first limit state, i.e. the appearance of the first cracks due to corrosion.

There are models based on a performance-based approach to predict the corrosion initiation phase, such as the fib model (fib Model-Code, 2010). These models were mostly developed from concretes made with Portland cement and binary binders. As a result, their predictions need some improvements when it comes to the impact of material properties (concretes with high replacements of clinker by MAs) and exposure conditions. It should also be emphasized that most of existing models only deal with the initial phase of corrosion.

The model shown below was developed by A. El Farissi (Farissi, 2020). It uses empirical laws derived from the exploitation of a database of 42 concretes of various mixture

proportions with various types of aggregates and MAs as part of a French National project (PerfDuB), as well as data from the literature, to quantify the phase of corrosion initiation and propagation(Carcasses et al., 2021).

3.1. Initiation period

The modeling procedure is explained in Figure 5. Diffusion is assumed to control the evolution of the carbonation depth (x_c) as a function of time, as done in most analytical carbonation models, such as the fib model (fib model-code 2010). As a result, the carbonation front x_c (mm) is expressed as a function of the square root of time (year$^{1/2}$) (equation 3):

$$x_c(t) = V_{NAT}\sqrt{t_{eff}} \quad (3)$$

Where :

$$V_{NAT} = V_{NAT,0}.k_{RH,ini} \quad (4)$$

V_{NAT} $(mm.year^{-1/2})$: the natural carbonation rate under actual environmental conditions (T, RH)

$V_{NAT,0}$ $(mm.year^{-1/2})$: the carbonation rate under reference conditions (T=20°C, RH=65%)

$k_{RH,ini}$: relative humidity parameter related to the corrosion initiation period

t_{eff} $(years)$: the effective carbonation time

Each term will be discussed and quantified separately in the following paragraphs.

Carbonation rate is influenced by both material properties and environmental factors. The model accounts for each parameter by decomposing each effect into distinct empirical functions. $V_{NAT,0}$ can be estimated from the results of an accelerated carbonation test because atmospheric carbonation is a long process. The accelerated carbonation test is described in section 2.2.1.a. An empirical relationship between natural carbonation rate under reference conditions $V_{NAT,0}$ (mm.year$^{-1/2}$) and accelerated carbonation rate V_{ACC} (mm.d$^{-1/2}$) could be determined from the PerfDuB database (equation 5).

$$V_{NAT,0} = 3.03V_{ACC} \quad (5)$$

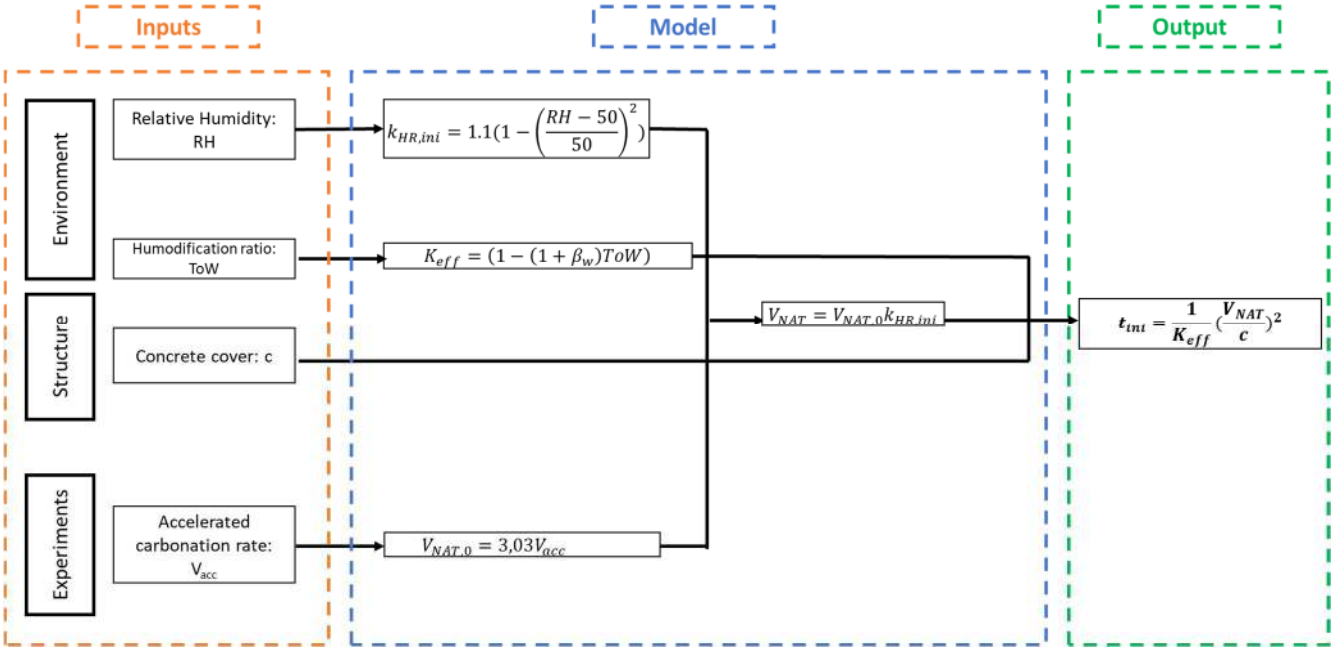

Figure 5: Diagram of the modelling procedure of the initiation period

The influence of ambient relative humidity on the initiation phase is expressed by $k_{RH,ini}$ (unitless). The carbonation rate is primarily controlled by the kinetics of chemical reactions at high RH and by the diffusion of CO_2 at low RH. Carbonation is assumed to be controlled by gas diffusion in the model proposed for carbonation. The effect of low RH cannot be taken into consideration with this model since we assume that the carbonation reaction is immediate. However, an empirical function is used to model the influence of RH over the entire range (0 to 100%) in a phenomenological approach (equation 6):

$$k_{RH,ini} = 1.1\left(1 - \left(\frac{\mathrm{RH} - 50}{50}\right)^2\right) \quad (6)$$

With RH the ambient relative humidity (%)

It should be noted that this empirical function is maximum at 50% RH, in the literature it has been shown that the RH leading to maximum carbonation rate can reach 60% (Wierig HJ, 1984). The function can be adapted if specific data on this maximum is available.

t_{eff} (year), the effective carbonation time: rain-induced wetting/drying cycles have a significant impact on the progress of carbonation front. When the surface of the material is saturated with rainwater, carbonation stops as the gaseous diffusion of CO_2 is not possible anymore. Then a drying phase is required so that the drying front exceeds Xc, allowing CO_2

diffusion and carbonation to proceed (R.F.M. Bakker, 1993). This slows down the carbonation process.

An effective carbonation time can be calculated based on this observation (equation 7).

$$t_{eff} = t - (t_w + t_d) = (1 - (1 + \beta_w)ToW)t = K_{eff}t \quad (7)$$

With

$$K_{eff} = (1 - (1 + \beta_w)ToW) \quad (8)$$

Where t the overall exposure time, t_w the total wetting time, and t_d the time it takes for the "drying front" to reach the carbonation front.

We assume that the relationship between t_d and t_w is linear to simplify this equation. These two times spans are actually tied to the same property: water permeability. t_d could be actually estimated with a drying model, as done in (Thiery et al., 2012) but this requires numerical resolution and the determination of water permeability determination which requires both additional experiments and numerical model (Poyet, 2013). Our objective was to design a relatively simple analytical model with a limited number of input parameters. This conservative approach results in the introduction of two parameters: a constant β_w, and the fraction of rainy days per year ToW (Time of Wetness).These recent findings originate from a study conducted by Vu et al. (Huy Vu et al., 2019) on 45 concretes exposed to natural carbonation over 5 years in various countries, whether shielded or not from the rain. β_w was found to be at least 1.5 from these data, and this is the value that was kept.

ToW depends on the exposure class: for classes XC1 to XC3, it is 0; for class XC4, it was set equal to 0.05.

Thus corrosion will be initiated when the carbonation front will reach the reinforcement front and therefore x_c=c, c being the concrete cover which is a structural parameter. By inverting equation 4, we obtain:

$$t_{ini} = \frac{1}{K_{eff}}\left(\frac{c}{V_{Nat}}\right)^2 \quad (9)$$

3.2. Propagation period

The modeling procedure is explained in Figure 6. The electrical resistivity of concrete has a direct impact on the corrosion process because it depicts the current flow between the anodic and cathodic regions. The association between electrical resistivity and corrosion rate has

been established; for a concrete with a high electrical resistivity, the corrosion current is low, and thus corrosion propagation is expected to be slower (Hornbostel et al., 2013).

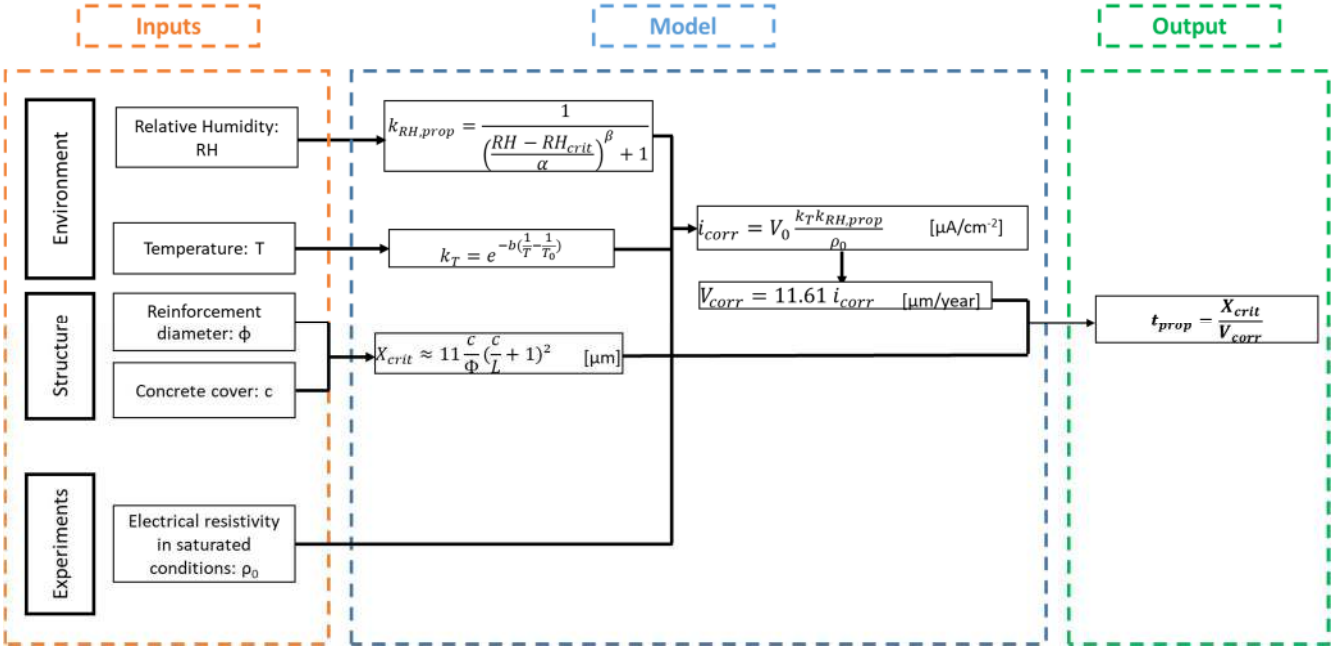

Figure 6: Diagram of the modelling procedure of the propagation phase

The equation 10 determines the time of corrosion propagation (t prop- [years]).

$$t_{prop} = \frac{X_{crit}}{V_{corr}} \quad (10)$$

where X_{crit} is the critical diameter loss for a crack opening of 0.1 mm and V_{corr} the corrosion rate. X_{crit} (m) was first proposed by Torres-Acosta et al (Torres-Acosta and Sagues, 2004) and it was calculated as follows: (equation 11).

$$X_{crit} \approx 11\frac{c}{\Phi}\left(\frac{c}{L} + 1\right)^2 \quad (11)$$

With :

c = concrete cover (mm)

Φ= reinforcement diameter (mm)

L = length of the anodic zone (mm).

Note that the concrete cover c is the same parameter as used in equation 9. In the case of carbonation, we consider uniform corrosion and therefore the ratio c/L is close to 0.

V_{corr} can be calculated as a function of the corrosion current density i_{corr} using equation 12 derived from Faraday's law (valid in the case of uniform corrosion) (François et al., 2018).

$$V_{corr} = \frac{\Delta s}{\Delta t} = \frac{M_{Fe}}{\rho s.F.z_a} i_{corr} = 11.61 i_{corr} \quad (12)$$

With V_{corr} (µm/year) the corrosion rate, Δs (m) the loss in diameter, Δt (s) the duration (s), M_{Fe} (56 g/mol) the molar mass of iron, ρs [g/m^3] the density of the steel, F the Faraday constant (96500 C), z the number of electrons exchanged at the anode and i_{corr} (µA/cm^2) the corrosion current density.

The corrosion current density is determined by an empirical formula obtained from the works of A. Farissi (Farissi, 2020) based on a bibliographic data analysis (Andrade et al., 1998) (equation 13).

$$i_{corr} = V_0 \frac{k_T.k_{RH,prop}}{\rho_0} \quad (13)$$

- V_0 (= 168.9 µA.Ωm.cm^{-2}) constant which reflects the corrosion potential, obtained from the analysis of literature data

- $k_{RH,prop}$ parameter which expresses the influence of RH on the propagation phase.

- k_T parameter which accounts for the influence of the temperature on the propagation phase.

- ρ_0 [Ω.m] the electrical resistivity of concrete in saturated conditions.

The temperature effect is taken into account using an Arrhenius law (equation 14) as it was done in (Jäggi et al., 2007), where T is the ambient temperature equal to the average annual temperature for a given environment (K), T_0 the reference temperature (293 K) and b is a regression constant equal to 4220 K.

$$k_T = e^{-b\left(\frac{1}{T}-\frac{1}{T_0}\right)} \quad (14)$$

For relative humidity, it is considered that the corrosion process in the case of carbonation has an optimum which corresponds to RH_{crit} for which the corrosion current density is maximum. Given the lack of consensus in the literature on the influence of relative humidity on the corrosion process and after exploitation of a large number of data from the literature

(Bouteiller et al., 2012; Stefanoni et al., 2018), the expression of $k_{HR,corr}$ was suggested (equation 15) where

$$k_{RH,corr} = \frac{1}{\left(\frac{RH - RH_{crit}}{\alpha}\right)^{\beta} + 1} \quad (15)$$

With:

RH: the relative humidity (%)

RHcrit: the critical relarive humidity which is considered equal to 95%

α and β : regression parameters.

Note that RH is the same parameter used to calculate $k_{RH,ini}$ in equation 7. In dry conditions (RH<60%) the corrosion is limited. It was found in (Stefanoni et al., 2018) that for HR=50% the corrosion current is actually reduced by a factor of 200. According to the authors, neither the electrochemistry of the corroding system nor kinetic restrictions resulting from the ohmic resistivity of the pore system nor restricted oxygen availability explain the substantial variation in the corrosion rate when changing RH but rather a surface effect which results from the wetting of the steel surface depending on the relative humidity in the concrete pore system. To take this effect into account, the parameters αand βare defined as follows:

$$\begin{array}{llll} HR \geq 60\% & \alpha = 6, & \beta = 2 \\ HR < 60\% & \alpha = 21, & \beta = 7 \end{array}$$

4- Results and discussion

4.1. Carbonation and its effects on microstructure

The carbonation of concrete is a physico-chemical process in which three mechanisms intervene:

- The diffusion of CO_2 inside the concrete, which depends on the transport properties,

- The dissolution of CO_2 and hydration products and their diffusion in the pore solution,

- The chemical reaction that produces calcium carbonates.

These mechanisms are summarized in the simplified Papadakis model (V. G. Papadakis et al., 1991) that allows, for a case of unidirectional diffusion of CO_2, to describe the progress of the carbonation front (equation 16):

$$x_c = \sqrt{\frac{2De_{CO_2}[CO_2]_0}{[CaO]_0}}\sqrt{t} \quad (16)$$

Where:

x_c: the carbonation front (mm)

De_{CO_2}: Effective diffusivity of CO_2 in carbonated concrete (m^2/s)

$[CO_2]_0$: The molar concentration of CO_2 per unit volume of the gas phase (mol/m^3)

$[CaO]_0$: The total molar concentration of carbonatable CaO (mol/m^3)

They are concomitant and the carbonation resistance of a material depends on both its physical and chemical properties. In this section the carbonation rate of the studied concretes is analyzed in the light of these properties.

Figure 7 shows the progress of the carbonation front of concretes II, III, C1 and C3 as a function of the square root of time. As a diffusive phenomenon, carbonation can be modeled by Fick's law. Under simplifying assumptions (V. Papadakis et al., 1991), the solution can be expressed in the form of equation 17:

$$x_c(t) = V_{ACC}\sqrt{t} \quad (17)$$

The curves were approximated by a linear curve. The R^2 of the four regressions were higher than 0.98. The table 6 summarizes the slopes of the curves that represent the accelerated carbonation rate of each concrete.

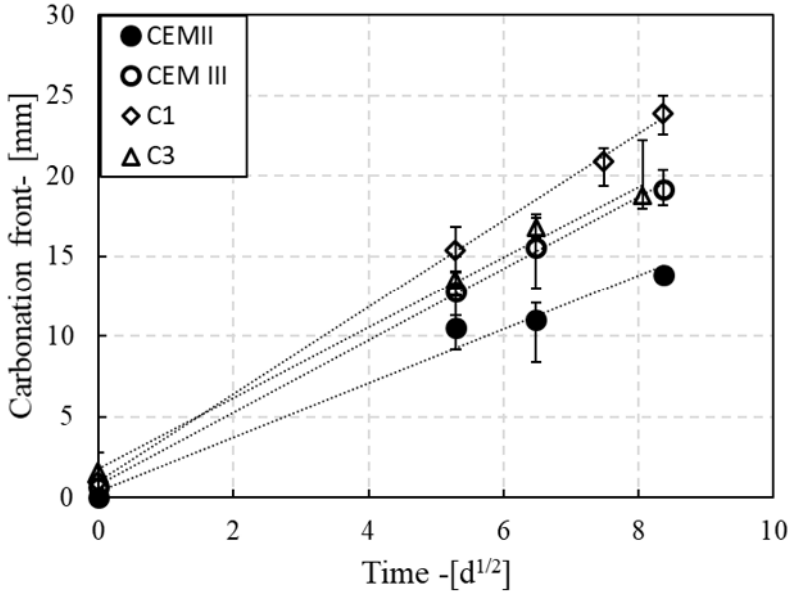

Table 6: Accelerated carbonation rates of the studied concretes

Concrete	V_{ACC} ($mm.t^{-1/2}$)
CEM II	1.67
CEM III	2.23
C1	2.70
C3	2.19

Figure 7: Accelerated carbonation depths of the studied concretes at 0, 28, 42 and 70 days

CEM II had the highest clinker content and it exhibited the highest carbonation resistance, C1 the lowest, and CEM III and C3 had approximately equal rates. A comparison between CEM III and C1, which have the same clinker content, reveals the negative effect of limestone on the carbonation resistance of the cement. The low carbonation rate observed for CEM II can be ascribed to his high clinker content, which results in higher content of carbonatable material thus higher carbonation resistance. This result is consistent with the findings of (Bolte et al., 2019) for the case of Clinker-Slag-Limestone ternary systems and (Medjigbodo et al., 2018) for Clinker-Metakaolin-Limestone systems.

From these data, the carbonation resistance of the studied concretes cannot be simply correlated with cement composition. As previously stated, the resistance to carbonation influences the initiation time of corrosion and, under specific RH conditions, the SL of concrete cover. The influence of microstructural properties and cement composition will be discussed from the experimental results in the following sections. Two microstructural variables may be relevant to investigate in order to understand concretes carbonation results: the chemistry of the microstructure and the PSD, which influences transport properties. We will first attempt to link carbonation resistance to microstructural features, then establish a link between cement composition and the microstructure of cementitious matrix.

a- Influence of the chemical parameters

CH content before carbonation and after 42 days of carbonation are shown in figure 8. The initial CH content of the various binders varies according to their initial composition; it depends on their clinker content and hydration reactions. After carbonation, the amount of CH consumed varied depending on cement paste initial composition. It was almost entirely consumed for cements with a low clinker content i.e. C1 and CEM III but significant CH content was observed for CEM II after carbonation.

To qualify the hydration products affected by carbonation as well as the carbonation products, XRD analyzes were carried out on C1 cement paste before and after carbonation; the results are shown in figure 9. Before carbonation, significant peaks of ettringite and carboaluminates can be observed. This is due to the presence of calcium carbonates which favors the stabilization of ettringite and hinders AFm formation (Adu-Amankwah et al., 2017). The peak of hemicarboaluminates is preponderant compared to monocarboaluminates. At high carbonate to aluminate ratios, the most stable form of the carboaluminates is

monocarboaluminate (Lothenbach, 2010), and this reaction consumes the portlandite and the calcite present in the limestone (Antoni et al., 2012).

After carbonation, TGA show that the portlandite is partially consumed for all the cement pastes, this observation is validated by XRD analysis on C1 (figure 9 –b). C-S-H being an amorphous phase, its presence is detected by a large bump around $2\theta=30°$. This bump flattened after carbonation, which indicates C-S-H carbonation. This reaction results in the formation of vaterite which is detected in carbonated cement paste spectrum (Morandeau et al., 2014). Ettringite was also partially consumed by carbonation. This reaction releases water and leads to the formation of aragonite (Nishikawa et al., 1992). Furthermore, there is a significant reduction in the amplitude of the hemicarboaluminate peak, this may be due either to their carbonation or to their transformation into monocarboaluminates given the formation of calcium carbonates resulting from the carbonation of portlandite and other hydrated phases.

Several authors have shown the influence of the initial CH content on the resistance to carbonation (Bucher et al., 2017). CH actually has a buffering effect which allows maintaining a high pH and promotes reinforcements depassivation. Shi et al (Shi et al., 2016) claim that the pH drop after carbonation is not only due to CH carbonation but also to C-S-H carbonation, especially high-Ca C-S-H. Since three studied binders are rich in GGBS, CH is consumed by GGBS hydration to form C-(A)-S-H. The model proposed by Papadakis (equation 16) actually states that the resistance to carbonation reflected by the carbonation front depends on the carbonatable products which include the C-S-H, ettringite, carboaluminates and other hydration products as well as some anhydrous phases (Shi et al., 2016). Figure 10 actually shows a inverse relationship ($R^2=0.97$) between the carbonation rate and all the hydrates formed which can be quantified from TGA by $BW_{40\text{-}550}$.

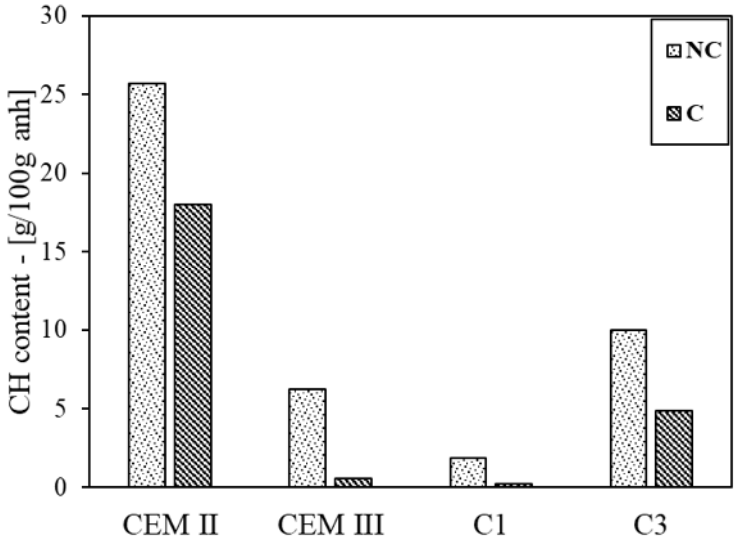

522

523 **Figure 8: Portlandite and bound water ($BW_{40\text{-}400°C}$) content of carbonated and non carbonated**
524 **cement pastes. NC is for non carbonated and C is for carbonated cement paste**

525

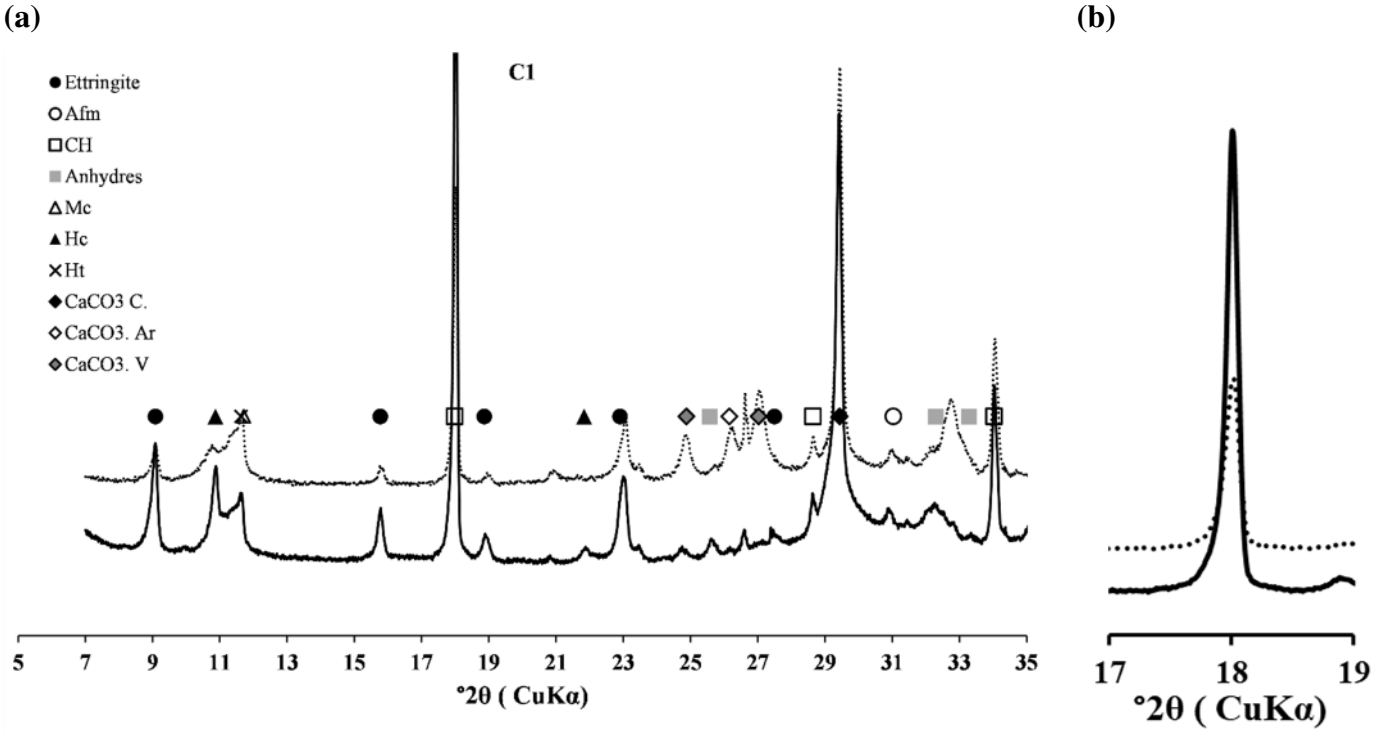

526 **Figure 9: (a) Influence of the carbonation on the microstructure of C1 cement paste (b)**
527 **Portlandite peak before and after carbonation. Solid line for non carbonated, and dashed line**
528 **for carbonated cement paste. AFm: monosulfoaluminate, CH: portlandite, Mc: monocarbonate,**
529 **Hc: Hemicarbonate, Ht: hydrotalcite, $CaCO_3$ C: calcite, Ar: aragonite, V: vaterite**
530

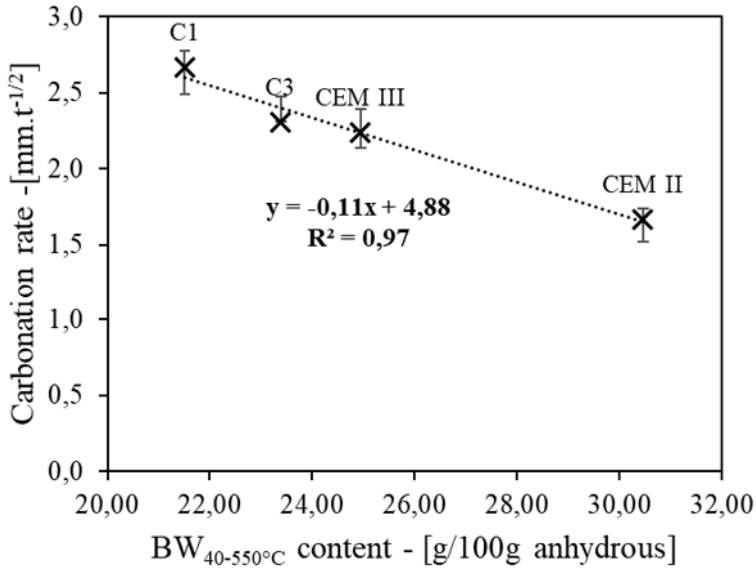

531

532 **Figure 10: Influence of total bound water on the carbonation rates of studied concretes**

533

534 b- Influence of the physical parameters

535 The PSD of carbonated and non-carbonated concrete cubes in figure 11 show that before
536 carbonation, the critical pore size decreased when increasing GGBS fraction.

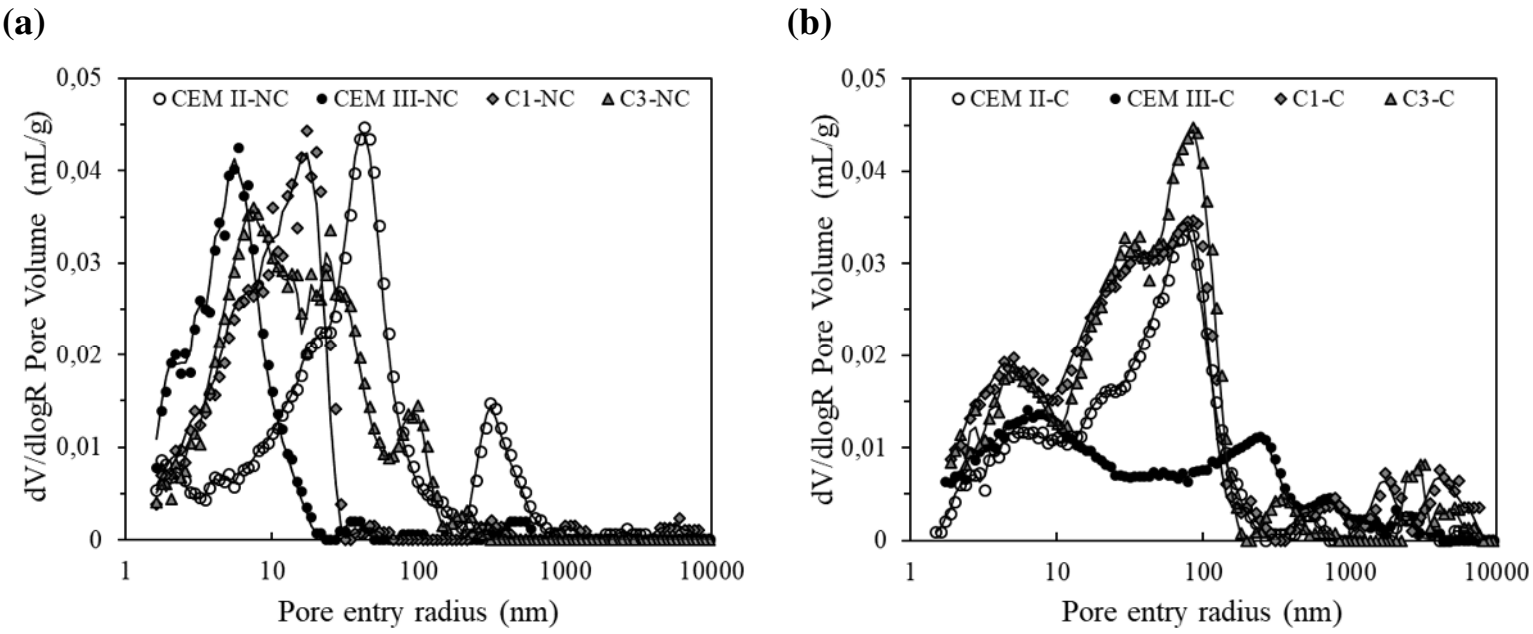

537 **Figure 11: Differential pore size distribution of (a) non carbonated (NC) and (b) carbonated (C)**
538 **concrete cubes**

539

The same trend has already been reported in [28]. After carbonation, the peaks are approximately at the same pore size, which is around 80nm except for CEM III which present two peaks, at 6 and 250nm. As shown in figure 8 CEM III cement paste actually had low CH content at later age and given its mineralogical composition, it had lower calcium to silicate (C/S) ratio than CEM I. These conditions allow: 1- C-S-H carbonation which leads to silica gel formation and therefore coarsens the microstructure (Gruyaert et al., 2013), and 2- ettringite carbonation which releases a lot of water (Nishikawa et al., 1992). In order to understand the effect of the carbonation of hydrates such as CH on the evolution of the pore size, the difference in the threshold radius before and after the carbonation has been plotted as a function of the quantity of carbonated CH expressed as the difference between the CH content before and after carbonation (cf figure 12).

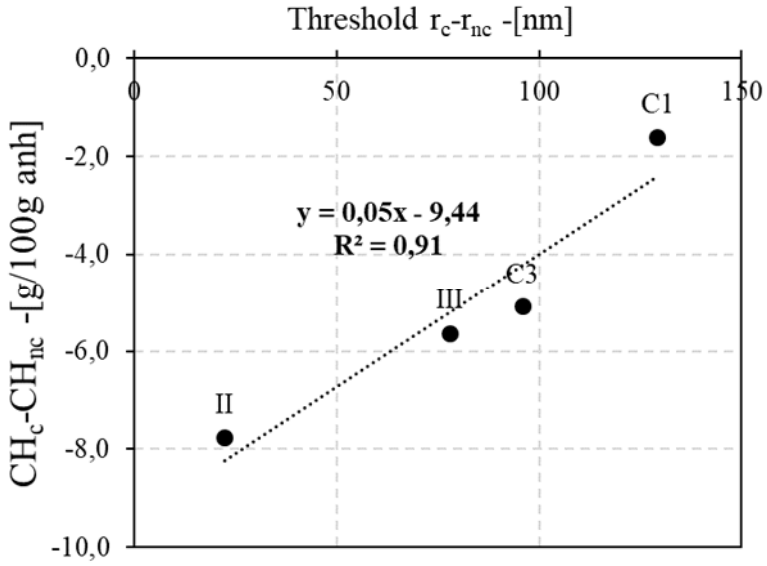

Figure 12: Correlation between the change in threshold pore size before and after carbonation and the portlandite content consumed by carbonation. r_c and r_{nc} represent radii of carbonated and non carbonated samples respectively.

Irrespective of the amount of CH consumed by carbonation, the difference in pore size before and after carbonation is positive. For CEM II, this difference is very small (<0.05µm). Furthermore, the higher the increase in the size of the pore radii, the lower the CH consumed by carbonation was, this suggests that it is not the carbonation of CH that is responsible for this increase in pore size, but rather the other hydrates. For the other cements, there was a higher coarsening of the pores, this can be explained by two factors: 1- The carbonation of C-(A)-S-H which produces silica gel and less stable polymorphs of calcium carbonates and

ettringite which releases a lot of water, 2- Carbonation shrinkage that occurs at the level of the pores. In fact, the latter results in decalcification and polymerization of C-S-H followed by formation of amorphous silica (Kangni-Foli et al., 2021). For ternary cements for whom little CH is available for carbonation, the PSD is negatively influenced. A similar result was observed in (Shah et al., 2018) for cement pastes made of clinker, metakaolin which has a pozzolanic activity, and limestone. This confirms the observations of Kangni-Foli et al. (Kangni-Foli et al., 2021) who found that carbonation of C-S-H leads to pore size coarsening. It was also found in the same study that the carbonation shrinkage of C-S-H pastes is more pronounced than that of C_3S paste and CH, this may further coarsen even more the microstructure. The authors also concluded that the lower carbonation resistance of some blended cement pastes was due to an increase in CO_2 diffusion coefficient induced by microcracking.

Ettringite crystals tend to grow in a direction that is less constrained by solid pores, such as into or around the pores rather than within the solid matrix (directed or non-directed). This crystal development in solid pores can substantially reduce the diameter of micro pores. Furthermore, after carbonation, ettringite is dehydrated and thus its crystals suffer a significant change in a and c lattice parameters, resulting in a decrease in crystal volume (Chen et al., 2019). As a result, the size and volume of pores containing ettringite might be increased.

In response to the first question concerning the link between the composition of cement and its resistance to carbonation, a good correlation was found between the rate of accelerated carbonation and the total bound water content of cements (figure 10). Calcium is present in almost all the hydrated phases and it mainly comes from the initial CaO present in the cement and GGBS. In (Shah et al., 2018) the author assumes that only the CaO contained in the clinker is able to bind CO_2. In our study, the active CaO content was calculated as the sum of the CaO contained in the clinker and the GGBS, as the GGBS has latent hydraulic properties which are activated by the hydration of the clinker (Roy and Idorn, 1982). Figure 13 shows a good correlation between the initial content of active CaO and the bound water content of long-term hydrated cement paste, which provides information on the CO_2 binding capacity of binary and ternary cements.

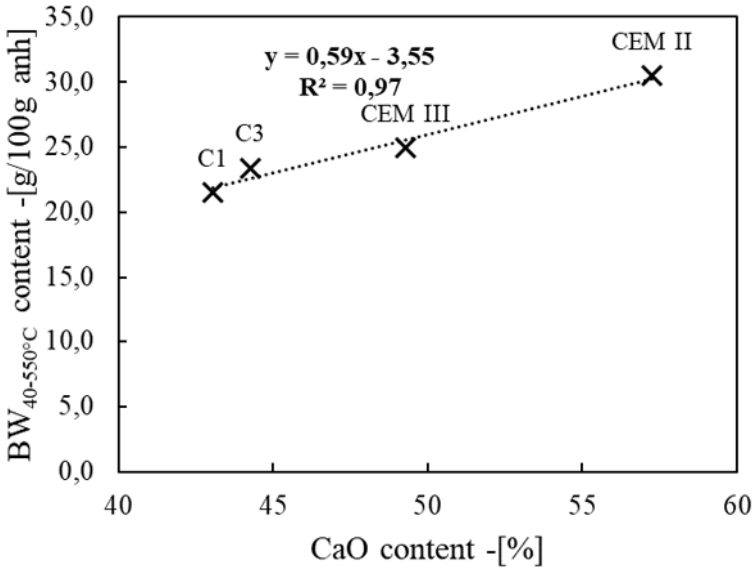

Figure 13: Correlation between total bound water content of mature cement pastes and initial reactive CaO content

4.2. Electrical resistivity

To standardize the results, the resistivity value retained for each sample corresponds to the slice closest to the center of the cubic sample. The figure 14-a shows the resistivity values plotted as a function of the threshold pore radius. CEM III and C1 had the same clinker content, and their values of electrical resistivity were very close, the difference could not be significant since the error bars overlap. In general, limestone does not have the same refinement effect on the microstructure as GGBS. A high clinker replacement by limestone has been reported to result in increased porosity in (Palm et al., 2016). Moreover, the pore solution composition has also an effect on concrete resistivity. It has been found that the cements containing pouzzolanic MAs are characterized by a lower alkalinity, since the alkali are bound in the C-S-H (Vollpracht et al., 2016). This results in high resistivity values, as observed in Chopperla et al. (Chopperla and Ideker, 2022) for the case of GGBS cement-based materials. Since limestone has a long-term diluting effect (Mounanga et al., 2011), its alkalinity-reducing effect may be insignificant.

The plot of electrical resistivity versus the threshold pore entry radius shown in figure 14-a reveals an exponential relationship and figure 14-b shows a strong correlation between threshold pore radius and GGBS content of the cements. This is in accordance with what has

been found in (Medeiros-Junior and Lima, 2016). For a given concrete mixture, GGBS content of cement appeared as a good indicator of corrosion propagation time as it gives information about relative variations of electrical resistivity. However, it has been found that the GGBS source may strongly influence the electrical resistivity (van Noort et al., 2016). Otieno et al, (Otieno et al., 2014) have also found that the oxydes composition of slag negatively influences the chloride penetration resistance of concrete since it affects the refinement of concrete microstructure. Thus, since there is a correlation between chloride diffusion coefficient and electrical resistivity (Chidiac and Shafikhani, 2020) this confirms the findings of (Van Noort et al., 2016).

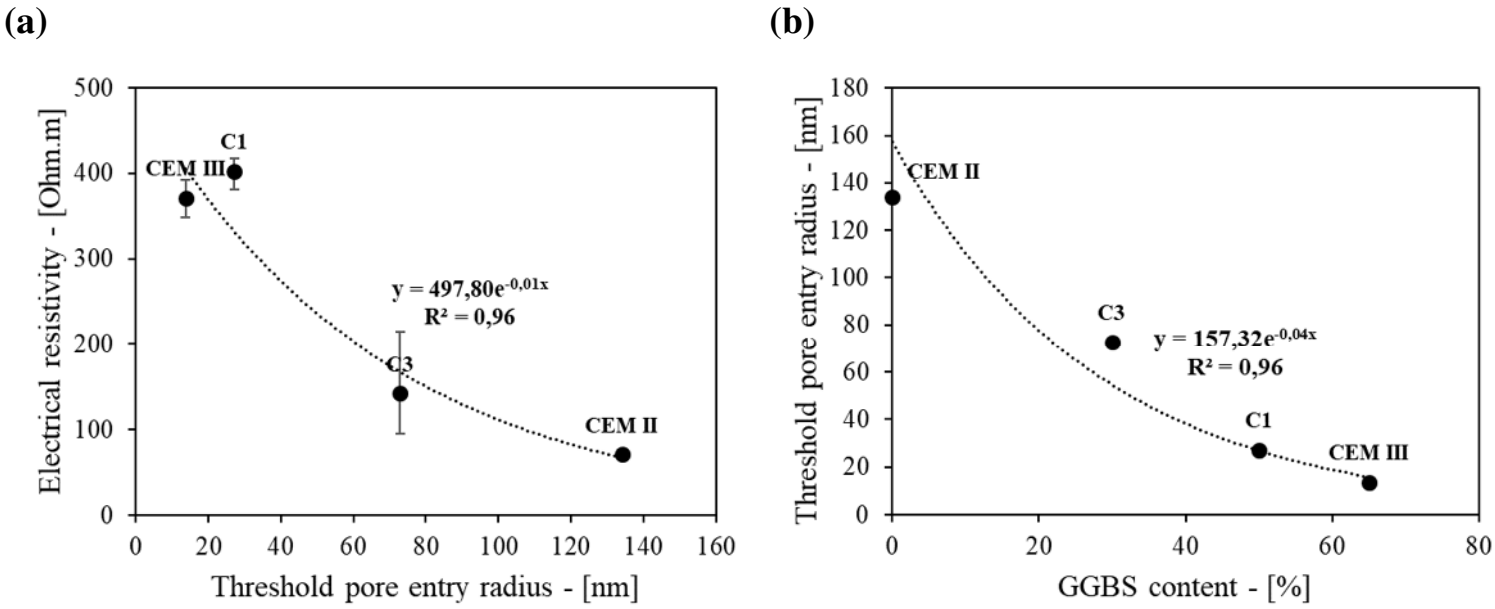

Figure 14: Correlation between (a) electrical resistivity and threshold pore radius and (b) threshold pore radius and GGBS content of the studied concretes

4.3. Service life prediction

The service life values given in this section correspond to the sum of initiation and propagation times of carbonation-induced corrosion. The prediction model is used to assess the influence of the main material properties used to characterize each process, respectively accelerated carbonation resistance and resistivity, on the total service life. The environmental conditions correspond to the XC exposure classes. The 4 subclasses XC1-XC4 are defined depending on the specific RH and rain conditions. The effects of temperature and curing conditions are out of the scope of this study. Table 7 describes the input data of RH and ToW (Time of Wetness i.e. the fraction of annual rainy days) for the 4 exposure classes. The cover

values taken for each exposure class are those recommended by Eurocode 2 for buildings and SL of 50 years. These values correspond to the minimum cover value (c_{min}) required by this standard, but in reality, an allowance in design for deviation (Δc_{dev})of 10mm is applied for cast-in-situ concrete, it is mentioned in the reinforcement design to take into account the possible movements of the reinforcements in the formwork at the time of implementation, the sum of the minimum cover value and the allowance in design for deviation is the nominal cover ($c_{nom} = c_{min} + \Delta c_{dev}$). The reinforcements diameter has been set at 20mm, which is a common value in construction projects.

Table 7: Environmental conditions described by XC exposure class and minimum concrete cover recommended for each class in Eurocode 2

	RH (%)	ToW (-)	Minimum cover c_{min} (mm)
XC1	50	0	15
XC2	90	0	25
XC3	75	0	25
XC4	65	0.05	30

The isolines of concrete cover SL are shown in figure 15. The duration presented is the sum of the corrosion initiation and propagation times ($t_{SL}=t_{ini}+t_{prop}$). The experimental results were used to predict the SL of the studied concretes for the different exposure classes. CEM III and CEM II are denoted in the graph by “III” and “II” respectively. It is noteworthy that the studied concrete mixtures comply with the requirements of standard EN 206 for an exposure class XC3/XC4 with regard to the minimum cement content and the maximum W/C ratio, and consequently they also comply with XC1 and XC2 classes which are less demanding. In addition, the mixture proportions and constituents of studied concretes were close to the concretes of the database of PerfDuB project concretes, which was used to establish the empirical laws of the model.

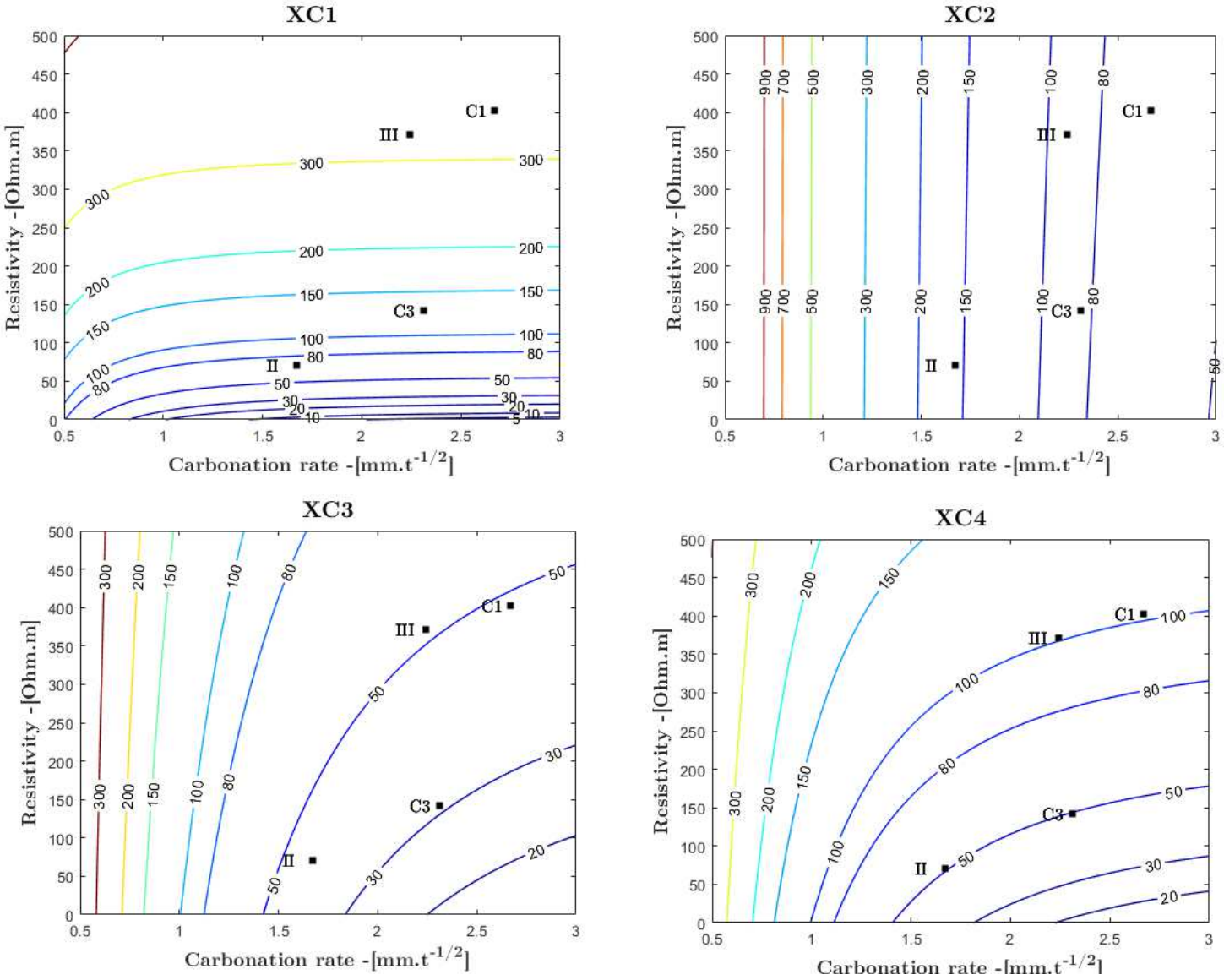

660 **Figure 15: Service life duration isolines in years predicted by the model for XC exposure classes**

661

662 The results of the sensitivity study on the cover value (Figure 16) show that for the most
663 demanding classes, namely XC3 and XC4, taking into account the safety margin clearly
664 improves the service life of the concrete cover and makes it possible to reach the target
665 lifetime for the structural class considered for all the concretes studied.

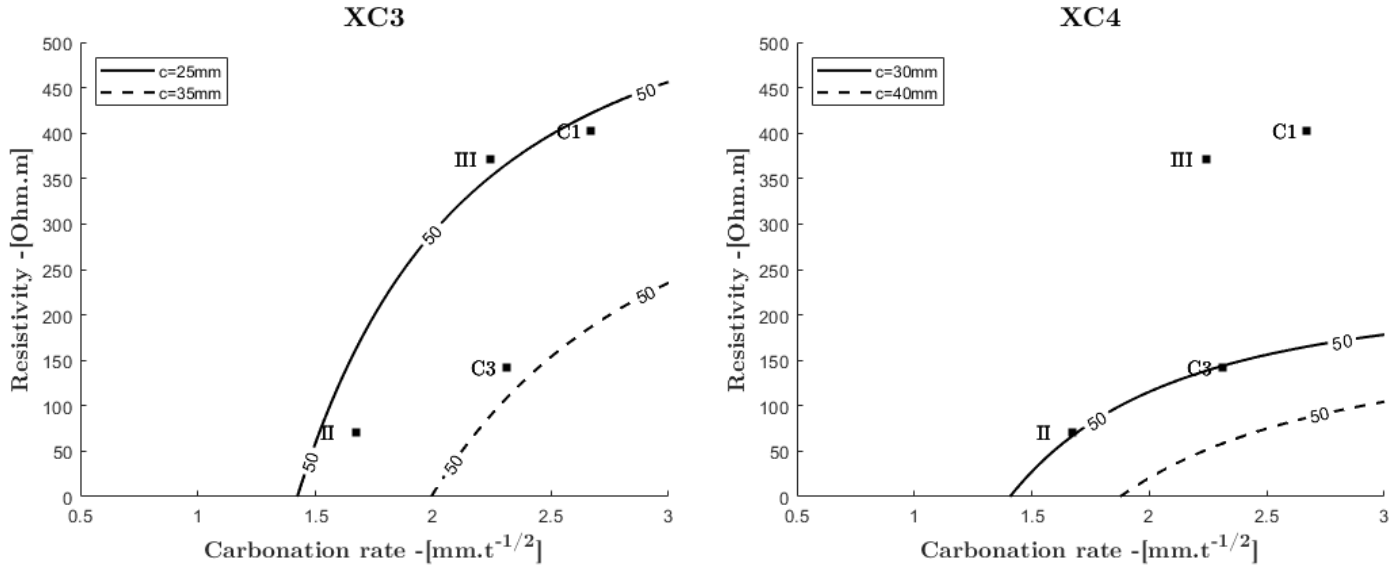

Figure 16: Sensitivity study of the concrete cover depth value for 50 years service life: minium cover c_{min} (solid lines) and nominal cover c_{nom} (dotted lines)

For XC1, the model predicts very long service lives and the iso-SL curves are almost parallel to the abscissa axis. Since the resistivity is much lower, the propagation time is much higher than the initiation time which becomes almost negligible ($t_{SL} \approx t_{prop}$). For all the studied concretes, the model predictions exceed 150 years, which is beyond the target SL for buildings (50 years). This reflects the relatively low corrosion risk in XC1 environments.

For XC2 class, the curves are almost parallel to the y-axis and slightly inclined. Considering the environmental conditions for this class (wet and very rarely dry), the corrosion is enhanced. Therefore, the time of propagation of corrosion is negligible compared to that of initiation ($t_{SL} \sim t_{ini}$).. Hence, the carbonation rate has a key role for this exposure class. In general, all the studied concrete covers have a SL duration of more than 50 years. High RH actually results in low carbonation rate.

For XC3 and XC4, the plots tend to be curved as the SL decreases; for concretes with low carbonation resistance, a high electrical resistivity significantly contributes to improving their SL, as is the case for C1 and CEM III (denoted III on the graph), which have a resistivity of the order of 400 Ohm.m. The curvature of the plots reflects the dominance of one phase over the other. For the domain of ρ and V_{ACC} presented in the graphs, the isolines begin to stabilize from V_{ACC} =1.25 for a SL of 50 years (in XC3), for the XC4 this can be observed for a Vacc < 1 mm.$d^{-1/2}$ for a SL of 100 year life.

From the results above, if the corrosion propagation time is taken into account, concretes made with ternary cements and relatively low resistance to carbonation can under certain

688 environmental conditions lead to more durable structures, as is the case for C1 for a XC1,
689 XC3 and XC4 classes.

690 4.4. CO_2 efficiency indicator (CO_2/Service Life)

691 In order to assess the environmental impact of these new cements, a calculation of CO_2
692 emissions was carried out. This calculation is based on the emission factors of the various
693 constituents (clinker, GGBS, limestone) collected from LCA analyses and environmental
694 product declaration (EPD)(AFNOR, 2014). The clinker data were provided by French
695 Technical Association of Hydraulic Binders (ATILH) for the year 2017. Emission factors for
696 each component are given in table 8. It is noteworthy to mention that the clinker emission
697 factors are not universal, but rather based on specific production process used in France. This
698 value could vary, for example, if clinker was produced using either fossil fuels or nuclear
699 energy as energy sources.

700 **Table 8: CO_2 emission factors used for the environmental analysis**

	Emission factor (kg CO_2/kg)		Reference
Clinker	0.881		(ATILH, 2017)
GGBS	with allocation(*)	0.114	(Chen et al., 2010)
	without allocation	0.085	(Miller, 2018)
Limestone	0.0278		(Proske et al., 2018)
Sand	0.0026		(Bolte et al., 2019)
Gravels	0.0075		(Wang and Lee, 2019)
Superplasticizer	0.767		(Miller, 2018)

701 (*) Economic allocation

702 These data were used to calculate the carbon emission of one cubic meter of concrete for each
703 cement studied. This emission was reported to the SL of the concrete cover predicted by the
704 model. This ratio, which is noted CO_2 efficiency indicator (CEI) is a more effective indicator
705 of the environmental impact of these cements since it provides information on the carbon cost
706 of one year of service of the concrete cover, which is proposed as a more representative
707 functional unit for the use of cement. Figure 17 shows the emission factors of the four studied
708 cements as well as their CEI for the composition of the concrete studied for exposure classes
709 XC1-XC4. The values presented are calculated for an average GGBS emission factor. The

error bars reflect whether or not the carbon allocation of the GGBS has been taken into account.

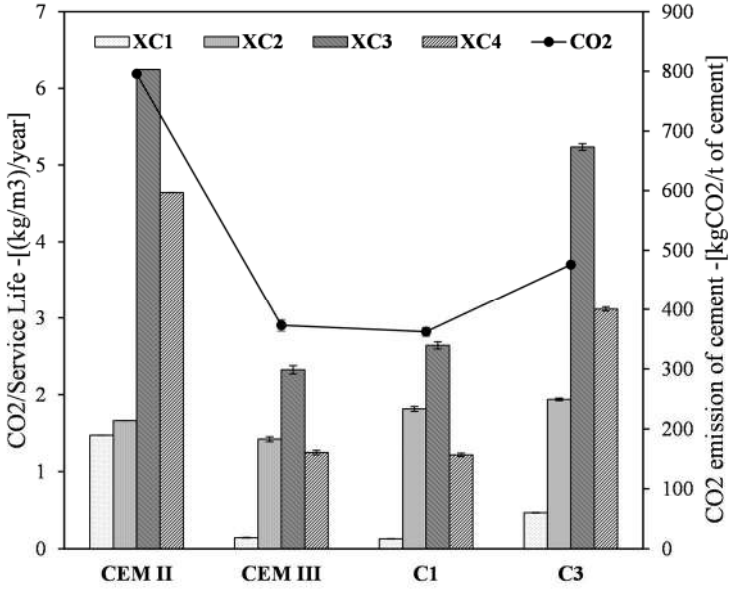

Figure 17: CO_2 emission factor and effective global warming potentiel (CEI) of the cements studied for XC1-XC4 exposure classes

A low CEI indicates a lower contribution of concrete production and use to climate change. CEM II, having a relatively high carbon footprint, has a relatively high CEI compared to other cements for almost all exposure classes except XC2 for which the initiation time prevails. CEM III, on the other hand, has a low CEI because there is a good compromise between his CO_2 emission and durability material properties. C1 show low CEI as well, in addition, this has the advantage of containing limestone, which is a natural resource that replace GGBS. GGBS is a more interesting MA since it is reactive in the long term (Giergiczny, 2019). Nevertheless, its carbon allocation is still questioned (Chen et al., 2010). GGBS is an industrial by-product and cannot be considered as waste since its production requires an investment to install granulators in iron manufacturing plants (Scrivener et al., 2018), in addition to the grinding, drying and filtration process necessary to make the product suitable for use in cement. Thus, depending on the carbon allocation of the GGBS, the CEI of these cements will evolve. Moreover, the importance of using GGBS efficiently given its limited availability has been highlighted in the study by Proske et al. (Proske et al., 2018) by introducing a “slag efficiency factor” into their analysis. Moreover, the difference in CEI is not very significant in the case of this study since the difference in the emission factor of the GGBS with and without allowance is not very large (table 8). Note that the allocation

considered is economic; the error bars for GGBS-containing cements could have been larger if another allocation type had been taken into account. Finally, the use of limestone presents an interesting prospect for partially replacing the GGBS in a ternary cement. Its environmental contribution is very low, and the results obtained show that, for a suitable concrete mixture, the material properties are good for an acceptable SL, on the other hand.

5- Conclusion

This paper is focused on the durability performance of concrete made with the ternary cements of the new European standard EN 197-5 relatively to their environmental impact. A new characterization of so-called "low-carbon cements" is proposed based on the CO_2 emission/service life of the concrete cover under carbonation induced corrosion which takes into account the propagation time as well as the initiation time. An experimental study aimed at determining the durability parameters of several concretes based on binary and ternary cements was carried out. An empirical model that takes into account both the initiation and propagation phases of corrosion process was used to predict the service life of the cover of the concretes studied from material properties. The findings of this study can be summed up as follows:

1- All the hydration products formed seem to contribute to the carbonation resistance of concretes
2- The initial reactive CaO content of cements, which comes from clinker and slag, provides information on the amount of water bound in the long term and thus it could be an indicator of the carbonation resistance for a given concrete mixture depending on the cement used.
3- The slag, by its positive influence on the refinement of the porosity, seems to have a significant effect on the extension of the corrosion propagation time as it contributes to the improvement of the electrical resistivity
4- The model used shows that the propagation duration can predominate over the initiation duration, especially under low relative humidity conditions, such as the environment described in the XC1 exposure class.
5- The new ternary binders seem to have a low CO_2 efficiency indicator (CEI) coefficient given their low carbon emission and acceptable service life. The combination of clinker, slag and limestone offer new possibilities in reducing the CO2 emissions of building materials while meeting the required durability.

765 Finally, since resistivity depends on the pore size and pore solution, it is interesting to explore
766 the evolution of the resistivity of concrete due to carbonation, as carbonation induces
767 modifications on those properties. This will allow a more precise and realistic prediction
768 given the chronology of the facts: the propagation of corrosion follows its initiation. Further
769 research would be necessary to draw clear conclusions on this issue.

770 CRediT authorship contribution statement

771 Imane Elkhaldi: Writing – original draft, Investigation, Visualization, Formal analysis
772 Emmanuel Roziere: Conceptualization, Methodology, Writing – review & editing,
773 Supervision
774 Philippe Turcry: Conceptualization, Writing – review & editing,
775 Ahmed Loukili: Conceptualization, Supervision, Funding acquisition, Project administration

776 Declaration of competing interest

777 The authors declare that they have no known competing financial interests or personal
778 relationships that could have appeared to influence the work reported in this paper.

779 Acknowledgements

780 The authors would like to thank EDYCEM company and Ecole Centrale de Nantes for their
781 financial support and ATILH (Association Technique de l'Industrie des Liants Hydrauliques –
782 French Technical Association of the Industry of Hydraulic Binders) for fruitful discussions.
783 Geraldine Villain from University Gustave Eiffel is also gratefully acknowledged for her
784 support in performing the resistivity tests.

785 References

786 Aboulayt, A., Jaafri, R., Samouh, H., Cherki El Idrissi, A., Roziere, E., Moussa, R., Loukili,
787 A., 2018. Stability of a new geopolymer grout: Rheological and mechanical
788 performances of metakaolin-fly ash binary mixtures. Constr. Build. Mater. 181, 420–
789 436. https://doi.org/10.1016/j.conbuildmat.2018.06.025
790 Adu-Amankwah, S., 2016. Relationship between Microstructure, Durability and Performance
791 of CEM X Composite Cements - PhD Thesis. The University of Leeds.
792 Adu-Amankwah, S., Zajac, M., Stabler, C., Lothenbach, B., Black, L., 2017. Influence of
793 limestone on the hydration of ternary slag cements. Cem. Concr. Res. 100, 96–109.
794 https://doi.org/10.1016/j.cemconres.2017.05.013
795 AFNOR, 2014. NF EN 15804+A1, Sustainability of construction works - Environmental
796 product declarations - Core rules for the product category of construction products.

Alonso, C., Andrade, C., González, J.A., 1988. Relation between resistivity and corrosion rate of reinforcements in carbonated mortar made with several cement types. Cem. Concr. Res. 18, 687–698. https://doi.org/10.1016/0008-8846(88)90091-9

Andrade, C., 2010. ELECTRICAL RESISTIVITY AS MICROSTRUCTURAL PARAMETER FOR THE MODELLING OF SERVICE LIFE OF REINFORCED CONCRETE STRUCTURES. 2nd Int. Symp. Serv. Life Des. Infrastruct. 10.

Andrade, C., Alonso, C., Sarría, J., 1998. Influencia de la humedad relativa y la temperatura en las velocidades de corrosión de estructuras de hormigón. Mater. Constr. 48, 5–17. https://doi.org/10.3989/mc.1998.v48.i251.468

Antoni, M., Rossen, J., Martirena, F., Scrivener, K., 2012. Cement substitution by a combination of metakaolin and limestone. Cem. Concr. Res. 42, 1579–1589. https://doi.org/10.1016/j.cemconres.2012.09.006

Arumugam, C., 2022. Polymer and non-polymer admixtures for concrete roofs: Thermal and mechanical properties, energy saving and carbon emission mitigation prospective. J. Build. Eng. 16.

ATILH, 2017. Déclaration Environnementale de Produit in French / Environnemental Product Declaration - CEM I.

Berodier, E., Scrivener, K., 2015. Evolution of pore structure in blended systems. Cem. Concr. Res. 73, 25–35. https://doi.org/10.1016/j.cemconres.2015.02.025

Bolte, G., Zajac, M., Skocek, J., Ben Haha, M., 2019. Development of composite cements characterized by low environmental footprint. J. Clean. Prod. 226, 503–514. https://doi.org/10.1016/j.jclepro.2019.04.050

Bouteiller, V., Cherrier, J.-F., L'Hostis, V., Rebolledo, N., Andrade, C., Victoire, E.M., 2012. Influence of humidity and temperature on the corrosion of reinforced concrete prisms. Eur. J. Environ. Civ. Eng. 16, 471. https://doi.org/10.1080/19648189.2012.668004

Bucher, R., Diederich, P., Escadeillas, G., Cyr, M., 2017. Service life of metakaolin-based concrete exposed to carbonation. Cem. Concr. Res. 99, 18–29. https://doi.org/10.1016/j.cemconres.2017.04.013

Carcasses, M., Cussigh, F., toutlemonde, F., 2021. Definition of performance thresholds according to exposure classes in french "Définition de seuils de performance en fonction des classes d'exposition."

Cardinaud, G., Rozière, E., Martinage, O., Loukili, A., Barnes-Davin, L., Paris, M., Deneele, D., 2021. Calcined clay – Limestone cements: Hydration processes with high and low-grade kaolinite clays. Constr. Build. Mater. 277, 122271. https://doi.org/10.1016/j.conbuildmat.2021.122271

Chen, B., Kuznik, F., Horgnies, M., Johannes, K., Morin, V., Gengembre, E., 2019. Physicochemical properties of ettringite/meta-ettringite for thermal energy storage: Review. Sol. Energy Mater. Sol. Cells 193, 320–334. https://doi.org/10.1016/j.solmat.2018.12.013

Chen, C., Habert, G., Bouzidi, Y., Jullien, A., Ventura, A., 2010. LCA allocation procedure used as an incitative method for waste recycling: An application to mineral additions in concrete. Resour. Conserv. Recycl. 54, 1231–1240. https://doi.org/10.1016/j.resconrec.2010.04.001

Chidiac, S.E., Shafikhani, M., 2020. Electrical resistivity model for quantifying concrete chloride diffusion coefficient. Cem. Concr. Compos. 113, 103707. https://doi.org/10.1016/j.cemconcomp.2020.103707

Chopperla, K.S.T., Ideker, J.H., 2022. Using electrical resistivity to determine the efficiency of supplementary cementitious materials to prevent alkali-silica reaction in concrete. Cem. Concr. Compos. 125, 104282. https://doi.org/10.1016/j.cemconcomp.2021.104282

Di Filippo, J., Karpman, J., DeShazo, J.R., 2019. The impacts of policies to reduce CO2 emissions within the concrete supply chain. Cem. Concr. Compos. 101, 67–82. https://doi.org/10.1016/j.cemconcomp.2018.08.003

du Plooy, R., Palma Lopes, S., Villain, G., Dérobert, X., 2013. Development of a multi-ring resistivity cell and multi-electrode resistivity probe for investigation of cover concrete condition. NDT E Int. 54, 27–36. https://doi.org/10.1016/j.ndteint.2012.11.007

EN 197-5:2021, CEN/TC 51, Cement — Part 5: Portland-composite cement CEM II/C-M and Composite cement CEM VI, 2021.

Farissi, A.E., 2020. Prédiction de la durée d'utilisation des ouvrages en béton armé par une approche performantielle dans le cas de la corrosion induite par la carbonatation ou l'attaque des ions chlorure in French / Prediction of the duration of use of reinforced concrete structures by a performance approach in the case of corrosion induced by carbonation or attack of chloride ions (phdthesis). Université de La Rochelle. https://doi.org/10/document

François, R., Laurens, S., Deby, F., 2018. Steel Corrosion in Reinforced Concrete, in: Corrosion and Its Consequences for Reinforced Concrete Structures. Elsevier, pp. 1–41. https://doi.org/10.1016/B978-1-78548-234-2.50001-9

Gartner, E., 2004. Industrially interesting approaches to "low-CO2" cements. Cem. Concr. Res. 34, 1489–1498. https://doi.org/10.1016/j.cemconres.2004.01.021

Giergiczny, Z., 2019. Fly ash and slag. Cem. Concr. Res. 124, 105826. https://doi.org/10.1016/j.cemconres.2019.105826

Gruyaert, E., Van den Heede, P., De Belie, N., 2013. Carbonation of slag concrete: Effect of the cement replacement level and curing on the carbonation coefficient – Effect of carbonation on the pore structure. Cem. Concr. Compos. 35, 39–48. https://doi.org/10.1016/j.cemconcomp.2012.08.024

Hope BB, Ip AKC, 1987. Corrosion of steel in concrete made with slag cement. ACI Mater J 525–31.

Hornbostel, K., Larsen, C.K., Geiker, M.R., 2013. Relationship between concrete resistivity and corrosion rate – A literature review. Cem. Concr. Compos. 39, 60–72. https://doi.org/10.1016/j.cemconcomp.2013.03.019

Huy Vu, Q., Pham, G., Chonier, A., Brouard, E., Rathnarajan, S., Pillai, R., Gettu, R., Santhanam, M., Aguayo, F., Folliard, K.J., Thomas, M.D., Moffat, T., Shi, C., Sarnot, A., 2019. Impact of different climates on the resistance of concrete to natural carbonation. Constr. Build. Mater. 216, 450–467. https://doi.org/10.1016/j.conbuildmat.2019.04.263

IPCC, 2022. Climate Change 2022: Mitigation of Climate Change. Contribution to the IPCC Sixth Assessment Report.

Jäggi, S., Böhni, H., Elsener, B., 2007. Macrocell corrosion of steel in concrete – experiments and numerical modelling, in: Corrosion of Reinforcement in Concrete. Elsevier, pp. 75–88. https://doi.org/10.1533/9781845692285.75

Kangni-Foli, E., Poyet, S., Le Bescop, P., Charpentier, T., Bernachy-Barbé, F., Dauzères, A., L'Hôpital, E., d'Espinose de Lacaillerie, J.-B., 2021. Carbonation of model cement pastes: The mineralogical origin of microstructural changes and shrinkage. Cem. Concr. Res. 144, 106446. https://doi.org/10.1016/j.cemconres.2021.106446

Kocaba, V., 2009. Development and evaluation of methods to follow microstructural development of cementitious systems including slags - PhD Thesis. Ecole Polytechnique Fédérale de Lausanne (EPFL).

Lothenbach, B., 2010. Thermodynamic equilibrium calculations in cementitious systems. Mater. Struct. 43, 1413–1433. https://doi.org/10.1617/s11527-010-9592-x

Lübeck, A., Gastaldini, A.L.G., Barin, D.S., Siqueira, H.C., 2012. Compressive strength and electrical properties of concrete with white Portland cement and blast-furnace slag. Cem. Concr. Compos. 34, 392–399. https://doi.org/10.1016/j.cemconcomp.2011.11.017

Markeset, G., Myrdal, R., 2008. Modeling of reinforcement corrosion in concrete - State of art (No. 7).

Matschei, T., Lothenbach, B., Glasser, F.P., 2007. The role of calcium carbonate in cement hydration. Cem. Concr. Res. 37, 551–558. https://doi.org/10.1016/j.cemconres.2006.10.013

Medeiros-Junior, R.A., Lima, M.G., 2016. Electrical resistivity of unsaturated concrete using different types of cement. Constr. Build. Mater. 107, 11–16. https://doi.org/10.1016/j.conbuildmat.2015.12.168

Medjigbodo, G., Rozière, E., Charrier, K., Izoret, L., Loukili, A., 2018. Hydration, shrinkage, and durability of ternary binders containing Portland cement, limestone filler and metakaolin. Constr. Build. Mater. 183, 114–126. https://doi.org/10.1016/j.conbuildmat.2018.06.138

Mehdipour, S., Nikbin, Iman.M., Dezhampanah, S., Mohebbi, R., Moghadam, H., Charkhtab, S., Moradi, A., 2020. Mechanical properties, durability and environmental evaluation of rubberized concrete incorporating steel fiber and metakaolin at elevated temperatures. J. Clean. Prod. 254, 120126. https://doi.org/10.1016/j.jclepro.2020.120126

Miller, S.A., 2018. Supplementary cementitious materials to mitigate greenhouse gas emissions from concrete: can there be too much of a good thing? J. Clean. Prod. 178, 587–598. https://doi.org/10.1016/j.jclepro.2018.01.008

Ministry for the ecological and solidary transition, 2020. National low carbon strategy-The ecological and inclusive transition towards carbon neutrality 176.

Morandeau, A., Thiéry, M., Dangla, P., 2014. Investigation of the carbonation mechanism of CH and C-S-H in terms of kinetics, microstructure changes and moisture properties. Cem. Concr. Res. 56, 153–170. https://doi.org/10.1016/j.cemconres.2013.11.015

Mounanga, P., Khokhar, M.I.A., El Hachem, R., Loukili, A., 2011. Improvement of the early-age reactivity of fly ash and blast furnace slag cementitious systems using limestone filler. Mater. Struct. 44, 437–453. https://doi.org/10.1617/s11527-010-9637-1

Nishikawa, T., Suzuki, K., Ito, S., Sato, K., Takebe, T., 1992. Decomposition of synthesized ettringite by carbonation. Cem. Concr. Res. 22, 6–14. https://doi.org/10.1016/0008-8846(92)90130-N

Otieno, M., Beushausen, H., Alexander, M., 2014. Effect of chemical composition of slag on chloride penetration resistance of concrete. Cem. Concr. Compos. 46, 56–64. https://doi.org/10.1016/j.cemconcomp.2013.11.003

Palm, S., Proske, T., Rezvani, M., Hainer, S., Müller, C., Graubner, C.-A., 2016. Cements with a high limestone content – Mechanical properties, durability and ecological characteristics of the concrete. Constr. Build. Mater. 119, 308–318. https://doi.org/10.1016/j.conbuildmat.2016.05.009

Papadakis, V., Vayenas, C., Fardis, M., 1991. Physical and Chemical Characteristics Affecting the Durability of Concrete. ACI Mater. J. 88, 186–196.

Papadakis, V.G., Vayenas, C.G., Fardis, M.N., 1991. Fundamental Modeling and Experimental Investigation of Concrete Carbonation. Mater. J. 88, 363–373. https://doi.org/10.14359/1863

Poyet, S., 2013. Determination of the intrinsic permeability to water of cementitious materials: Influence of the water retention curve. Cem. Concr. Compos. 35, 127–135. https://doi.org/10.1016/j.cemconcomp.2012.08.023

Proske, T., Rezvani, M., Palm, S., Müller, C., Graubner, C.-A., 2018. Concretes made of efficient multi-composite cements with slag and limestone. Cem. Concr. Compos. 89, 107–119. https://doi.org/10.1016/j.cemconcomp.2018.02.012

R.F.M. Bakker, 1993. Model to calculate the rate of carbonation resistance of conrete under different climatic conditions,. Rapp CEMIJ Bv Lab Imuiden Holl.

Roy, D.M., Idorn, G.M., 1982. Hydration, Structure, and Properties of Blast Furnace Slag Cements, Mortars, and Concrete. ACI J. Proc. 79. https://doi.org/10.14359/10919

Rozière, E., Loukili, A., Cussigh, F., 2009. A performance based approach for durability of concrete exposed to carbonation. Constr. Build. Mater. 23, 190–199. https://doi.org/10.1016/j.conbuildmat.2008.01.006

Scrivener, K.L., John, V.M., Gartner, E.M., 2018. Eco-efficient cements: Potential economically viable solutions for a low-CO2 cement-based materials industry. Cem. Concr. Res. 114, 2–26. https://doi.org/10.1016/j.cemconres.2018.03.015

Shah, V., Scrivener, K., Bhattacharjee, B., Bishnoi, S., 2018. Changes in microstructure characteristics of cement paste on carbonation. Cem. Concr. Res. 109, 184–197. https://doi.org/10.1016/j.cemconres.2018.04.016

Shi, Z., Lothenbach, B., Geiker, M.R., Kaufmann, J., Leemann, A., Ferreiro, S., Skibsted, J., 2016. Experimental studies and thermodynamic modeling of the carbonation of Portland cement, metakaolin and limestone mortars. Cem. Concr. Res. 88, 60–72. https://doi.org/10.1016/j.cemconres.2016.06.006

Stefanoni, M., Angst, U.M., Elsener, B., 2018. Electrochemistry and capillary condensation theory reveal the mechanism of corrosion in dense porous media. Sci. Rep. 8, 7407. https://doi.org/10.1038/s41598-018-25794-x

Thiery, M., Cremona, C., Baroghel-Bouny, V., 2012. Application of the reliability theory to the assessment of carbonation-induced corrosion risk of rebars. Eur. J. Environ. Civ. Eng. 16, 273–287. https://doi.org/10.1080/19648189.2012.667987

Torres-Acosta, A.A., Sagues, A.A., 2004. Concrete Cracking by Localized Steel Corrosion--Geometric Effects. Mater. J. 101, 501–507. https://doi.org/10.14359/13489

Turcry, P., J. Mai-Nhu, E. Rozière, B. Thauvin, F. Cussigh, 2019. French project “PerfDub” on performance-based approach: from Round-Robin tests to new test procedures for durability indicators and accelerated carbonation. Proc. Fib Symp. Concr. – Innov. Mater. Des. Struct. 505–512.

Tuutti, K., 1982. Corrosion of steel in concrete. Swed. Cem. Concr. Res. Inst. Stockh.

van Noort, R., Hunger, M., Spiesz, P., 2016. Long-term chloride migration coefficient in slag cement-based concrete and resistivity as an alternative test method. Constr. Build. Mater. 115, 746–759. https://doi.org/10.1016/j.conbuildmat.2016.04.054

Vollpracht, A., Lothenbach, B., Snellings, R., Haufe, J., 2016. The pore solution of blended cements: a review. Mater. Struct. 49, 3341–3367. https://doi.org/10.1617/s11527-015-0724-1

Wang, X.-Y., Lee, H.-S., 2019. Effect of global warming on the proportional design of low CO2 slag-blended concrete. Constr. Build. Mater. 225, 1140–1151. https://doi.org/10.1016/j.conbuildmat.2019.07.134

Wierig HJ, 1984. Longtime studies on the carbonation of concrete under normal outdoor exposure. In: Proceedings of the RILEM seminar on the durability of concrete structures under normal outdoor exposure 239–49.

Yang, K.-H., Jung, Y.-B., Cho, M.-S., Tae, S.-H., 2017. Effect of Supplementary Cementitious Materials on Reduction of CO2 Emissions From Concrete, in: Handbook of Low Carbon Concrete. Elsevier, pp. 89–110. https://doi.org/10.1016/B978-0-12-804524-4.00005-1